iScience

CellPress
OPEN ACCESS

Article

Alternately Dipping Method to Prepare Graphene Fiber Electrodes for Ultra-high-Capacitance Fiber Supercapacitors

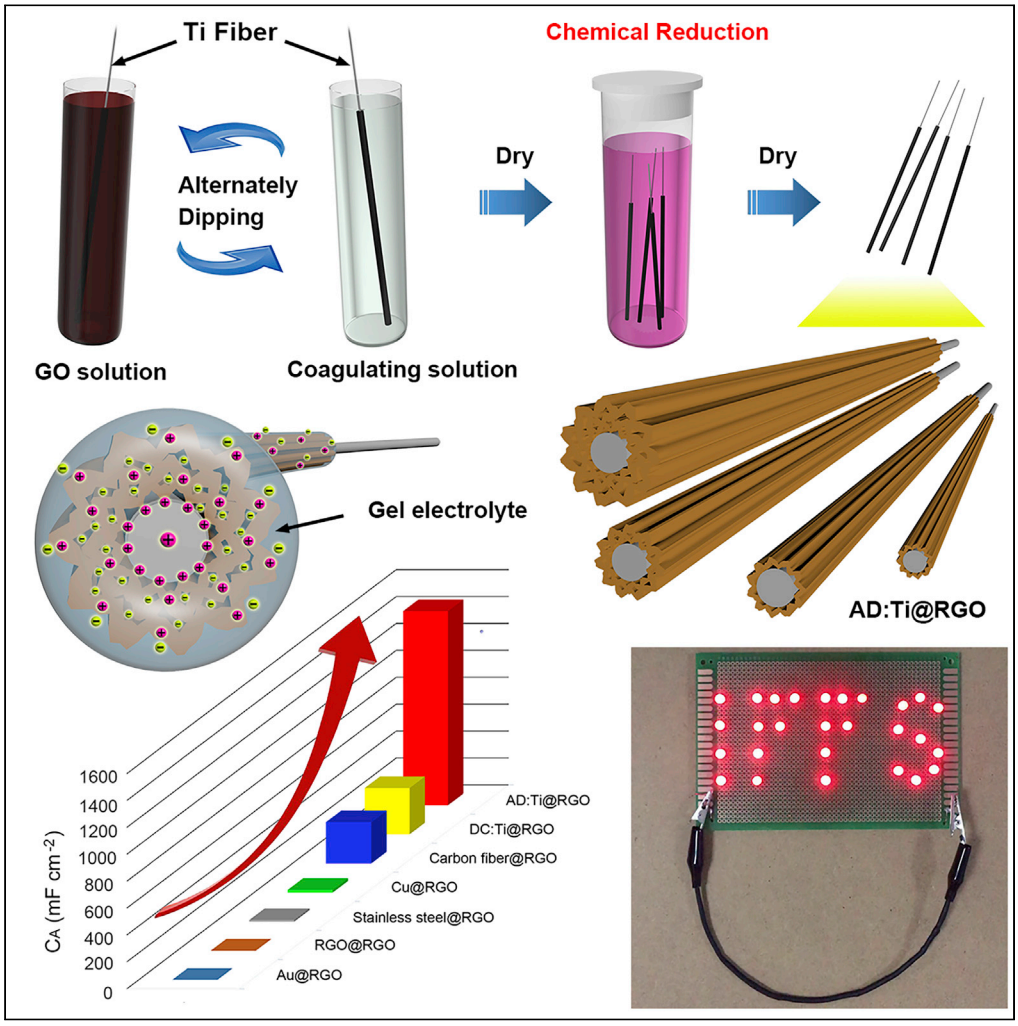

Guoxing Qu, Yu Zhou, Jiahao Zhang, Lei Xiong, Qin Yue, Yijin Kang

kangyijin@uestc.edu.cn

HIGHLIGHTS

A novel alternately dipping method to fabricate graphene fibers is reported

This method brings the fibers excellent mechanical and electrochemical properties

The graphene fiber shows an ultra-high specific capacitance of 1,722.1 mF cm^{-2}

Qu et al., iScience 23, 101396
August 21, 2020
https://doi.org/10.1016/j.isci.2020.101396

iScience

CellPress
OPEN ACCESS

Article

Alternately Dipping Method to Prepare Graphene Fiber Electrodes for Ultra-high-Capacitance Fiber Supercapacitors

Guoxing Qu,[1] Yu Zhou,[1] Jiahao Zhang,[1] Lei Xiong,[1] Qin Yue,[1] and Yijin Kang[1,2,*]

SUMMARY

Flexible fiber supercapacitors are promising candidate for power supply of wearable electronics. Fabrication of high-performance fibers is in progress yet challenging. The currently available graphene fibers made from wet-spinning or electro-deposition technologies are far away from practical applications due to their unsatisfactory capacitance. Here we report a facile alternately dipping (AD) method to coat graphene on wire-like substrates. The excellent mechanical properties of the substrate with greatly diverse choices can be carried over to the fiber supercapacitors. Under such guideline, the graphene fiber with a titanium core made by our AD method (AD:Ti@RGO) shows an ultra-high specific capacitance of up to 1,722.1 mF cm^{-2}, which is ~1,000 times that of wet-spinning- and electro-deposition-fabricated neat graphene fibers and presents the highest specific capacitance to date. With excellent mechanical properties and striking electrochemical performances, the AD:Ti@RGO-based supercapacitors light the path to the next-generation technologies for wearable devices.

INTRODUCTION

Wearable electronics, such as smart fabrics, wearable light-emitting diodes (LEDs), and implantable sensors are rapidly prevailing in contemporary high-tech era due to their attractive prospects for health monitoring, motion tracking, and ubiquitous access to information (Gao et al., 2016). These wearable electronics are being starved of flexible energy storage devices as power sources, among which the all-solid-state fiber supercapacitor (FSC) for its technical advantages in energy storage, knittability, integratability, and safety holds great promise (Chen et al., 2019). Pursuing high-performance FSCs, great efforts have been made on fibers to enable excellent flexibility, high tension strength, superior conductivity, and high capacitance. Carbon materials, metal (hydr)oxides, sulfides, conductive polymers, etc., have all been explored to be integrated into electrode fibers (Qu et al., 2016; Sumboja et al., 2013; Cao et al., 2015; Zhao et al., 2014). Whether as an active component or not, carbon materials are the most commonly used materials for the hosting matrix. Graphene has attracted wide attention for application in flexible electrode materials for a number of unique properties, such as extraordinary conductivity, high chemical stability, etc. (Huang et al., 2013; Li et al., 2013; Meng et al., 2013; Kim et al., 2010; Shao et al., 2015; Cao et al., 2014). Various methods have been reported to prepare graphene-based fibers, typically including wet-spinning and electro-deposition (Zhao et al., 2013; Kim et al., 2014).

Xu et al. fabricated neat graphene fibers by spinning aqueous graphene oxide (GO) in a coagulation bath (Xu and Gao, 2011). Because various compatible additives, such as MXene (Hu et al., 2017), polypyrrole (Xu et al., 2015; Huang and Kaner, 2004), and carbon nanotube (Ren et al., 2013), could be added into the GO precursor solution, wet-spinning technology is a scalable and universal approach to fabricate composite graphene-based fibers (Xu and Gao, 2015). The wet-spinning graphene-based fibers offer high flexibility and infinite length. Tensile force is inevitable for wearable device; however, wet-spinning graphene fibers usually have unsatisfactory fracture strength of lower than 150 MPa for the wearable applications (Xu and Gao, 2011, 2015). To address this issue, a general strategy is to coat graphene on strong fiber-like substrates. Au, Cu, and polymethyl methacrylate wires have been explored as substrate materials for graphene coating (Li et al., 2013; Huang et al., 2017a; Bae et al., 2011). Li et al. electrochemically prepared reduced graphene oxide (RGO) deposited on an Au wire for FSCs (Li et al., 2013). Electro-deposition could easily realize RGO deposited on metal wire and render the as-prepared fibers improved conductivity and tension

[1]Institute of Fundamental and Frontier Sciences, University of Electronic Science and Technology of China, Chengdu 610054, China

[2]Lead Contact

*Correspondence: kangyijin@uestc.edu.cn

https://doi.org/10.1016/j.isci.2020.101396

strength. However, the practical application of electro-deposition is limited for the sustained disadvantages, including unscalable production and restraint of substrate selection to conductive wire only.

In terms of electrochemical property, neat graphene fibers prepared by both wet-spinning and electro-deposition show unsatisfactory charge-storage capability for the level of device application. Wet-spinning RGO fibers have a typical specific capacitance of 3.3 mF cm^{-2} (Huang et al., 2013), whereas the conventional electro-deposition RGO fibers show a specific capacitance of only 0.7–1.7 mF cm^{-2} (Li et al., 2013; Meng et al., 2013). Recently, Huang et al. (Huang et al., 2017a) modified the dimensionally confined (DC) method that was first reported by Dong et al. (Dong et al., 2012), by coating GO on the Cu wire to form Cu@RGO fibers, improving the capacitance to 20 mF cm^{-2}. Kouet al. improved the wet-spinning method to prepare polyelectrolyte-wrapped graphene/carbon nanotube core-sheath fibers with specific capacitance of up to 177 mF cm^{-2} (Kou et al., 2014). Nevertheless, the easy, efficient, and scalable fabrication of graphene fibers that have a high capacitance to meet the demand of flexible power supply in a wearable device remains challenging.

Herein, we report a novel alternately dipping (AD) strategy to fabricate graphene fibers by alternately dipping a fiber-like substrate in GO aqueous solution and coagulation solution. The fiber obtained through coating neat RGO on a titanium (Ti) wire by the AD method (denoted as AD:Ti@RGO) shows both excellent mechanical property and electrochemical performance. The assembled symmetric all-solid-state FSCs using the AD:Ti@RGO as electrodes show an extremely high charge-storage capability, cycling stability, and excellent resistance to bending fatigue. The AD:Ti@RGO-based FSCs reveal an ultra-high specific areal single-electrode capacitance of up to 1,722.1 mF cm^{-2} at a current density of 0.1 mA cm^{-2}, which is up to 1,000 times that of previously reported FSCs based on neat RGO fibers via wet-spinning and electro-deposition technology. To the best of our knowledge, it is the highest record for all-solid-state FSCs to date. Ultra-high energy density of 126.5 μW h cm^{-2} (or 22.9 mW h cm^{-3}) at power density of 83.0 μW cm^{-2} (or 15.0 mW cm^{-3}) is achieved. Moreover, the FSCs show an excellent cycling stability with capacitance retention of 96% after 10,000 cycles and a negligible capacitance fade even after bending 500 times. Based on the high performances of AD:Ti@RGO, wire-like supercapacitor bank devices are fabricated to power various electronics, demonstrating a promising prospect of practical application.

RESULTS

Fabrication and Characterization of the AD:Ti@RGO

The fabrication of AD:Ti@RGO is schematically shown in Figures 1A and S1A. To prepare AD:Ti@RGO, a clean Ti wire is alternately dipped in GO solution and the coagulating solution made of deionized water, ethanol, and sodium hydroxide (NaOH). As this AD cycle goes on, GO is coated on the Ti wire layer by layer due to the alignment and attachment of GO on the coagulation liquid-wetted surface (see Video S1). After drying, ascorbic acid (AA) dissolved in diluted coagulating solution is used to reduce the coating GO to RGO at 85°C. As described earlier, the AD method is facial, low cost, and scalable. For instance, it is easy to regulate the loading mass of RGO on a Ti wire by controlling the cycle number of the AD operation. Moreover, the fiber substrate is not limited to Ti wire. Various metal wires with different diameters, even the human hair, could serve as a substrate (Figures S1B–S1F). As the DC method is a widely adopted method to prepare graphene fibers with improved electrochemical performances, fibers of RGO coating on Ti wire by the DC method (denoted as DC:Ti@RGO) are also prepared for comparison purpose.

As shown in the scanning electron microscopic (SEM) images and photographs of the AD:Ti@RGO, RGO is uniformly coated on Ti wires (Figures 1B and S2A). A core-sheath structure of AD:Ti@RGO could be seen from the inset in Figure 1B. The corresponding high-magnification image (Figure 1C) reveals the substantially wrinkled surface of AD:Ti@RGO, which could greatly increase the electrode/electrolyte interfacial area and thus improve the electrical double-layer capacitance. A well-defined core-sheath structure of the AD:Ti@RGO can be further verified by the cross-sectional SEM image (Figure 1D). The high-magnification cross-sectional SEM image (Figure 1E) reveals that the RGO sheets in the AD:Ti@RGO are nematic and parallel to the substrate fiber axis. Such alignment of RGO sheets results from the flow-induced alignment of GO dispersions, as also observed in previous wet-spinning (Xu and Gao, 2015).

The Raman spectrum of the AD:Ti@RGO (Figure 1F) shows two peaks around 1,340 and 1,580 cm^{-1} that are assigned to the D and G bands of carbon, respectively Kudin et al., 2008, with an I_D/I_G value of 1.4, which is greater than that of RGO in previous reports Cao et al., 2013. With the same starting GO solution,

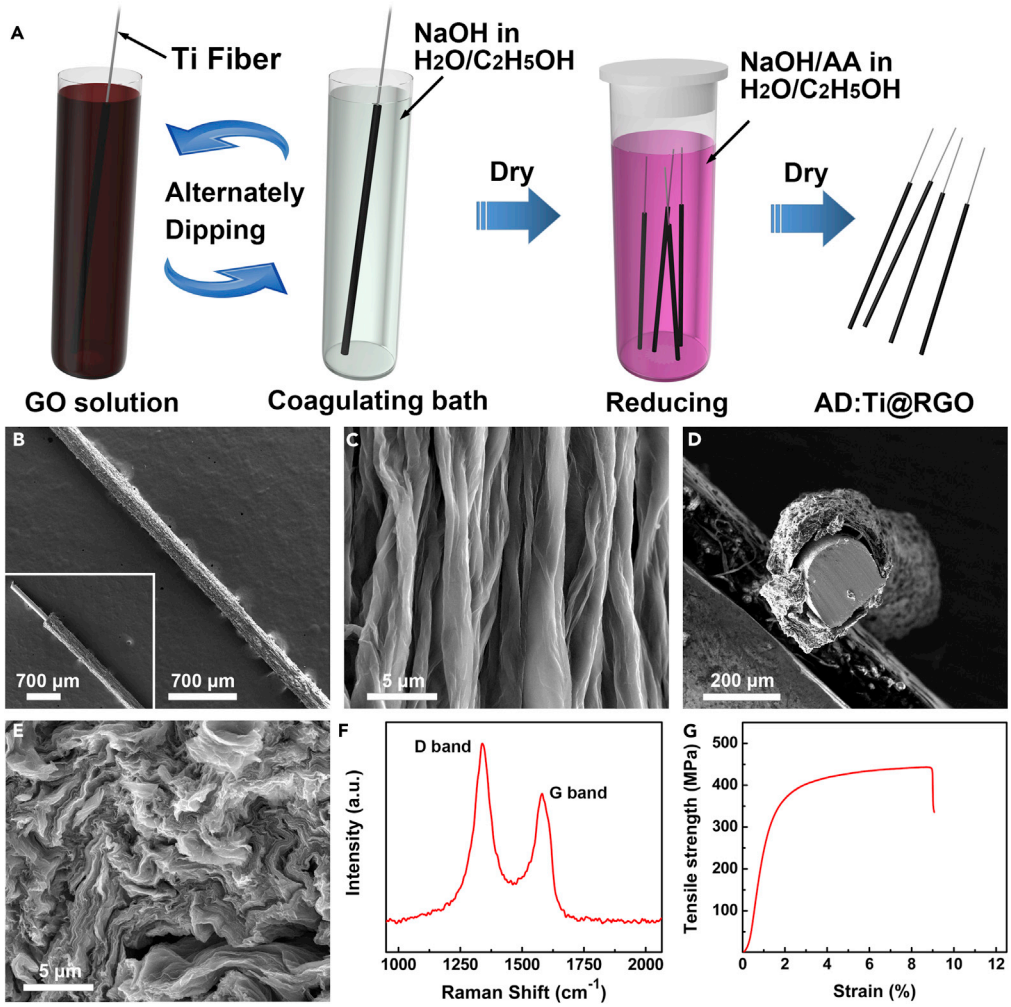

Figure 1. Fabrication and Characterization of the AD:Ti@RGO

(A) Schematic illustration of the AD:Ti@RGO preparation.

(B and C) (B) Low- and (C) high-magnification SEM images of the AD:Ti@RGO by side view. The inset shows the core-sheath structure of the AD:Ti@RGO.

(D and E) (D) Low- and (E) high-magnification cross-sectional SEM images of the AD:Ti@RGO.

(F) Raman spectrum of the AD:Ti@RGO.

(G) Typical stress-strain curve of the AD:Ti@RGO.

DC:Ti@RGO shows an I_D/I_G value of only 1.1 (Figure S3), indicating that the strong alkaline NaOH solution used in the AD approach may be responsible for the high population of defects (Chen et al., 2014a).

The AD:Ti@RGO possesses outstanding tensile strength as high as 443 MPa (Figure 1G), which is about three times that of wet-spinning neat RGO fiber. As some special Ti-based alloys may have even higher tensile strength (e.g., Ti-beta-C of 1,400 MPa), the fibers made with RGO on such alloys via AD approach are expected to carry over the extraordinary mechanical property of substrates. As the AD:Ti@RGO is flexible, it can adapt to any curved surface of human body, even on objects with a high curvature such as finger (Figure S2B). AD:Ti@RGO can be bent into a small circle or a spring, demonstrating an excellent flexibility that is suitable for wearable devices (Figures S2C and S2D).

Electrochemical Performances of the AD:Ti@RGO-Based FSCs

To investigate the electrochemical performances of the AD:Ti@RGO, symmetric all-solid-state FSCs are fabricated using an H_3PO_4/polyvinyl alcohol/H_2O gel electrolyte. Although Ni and Cu wires have been

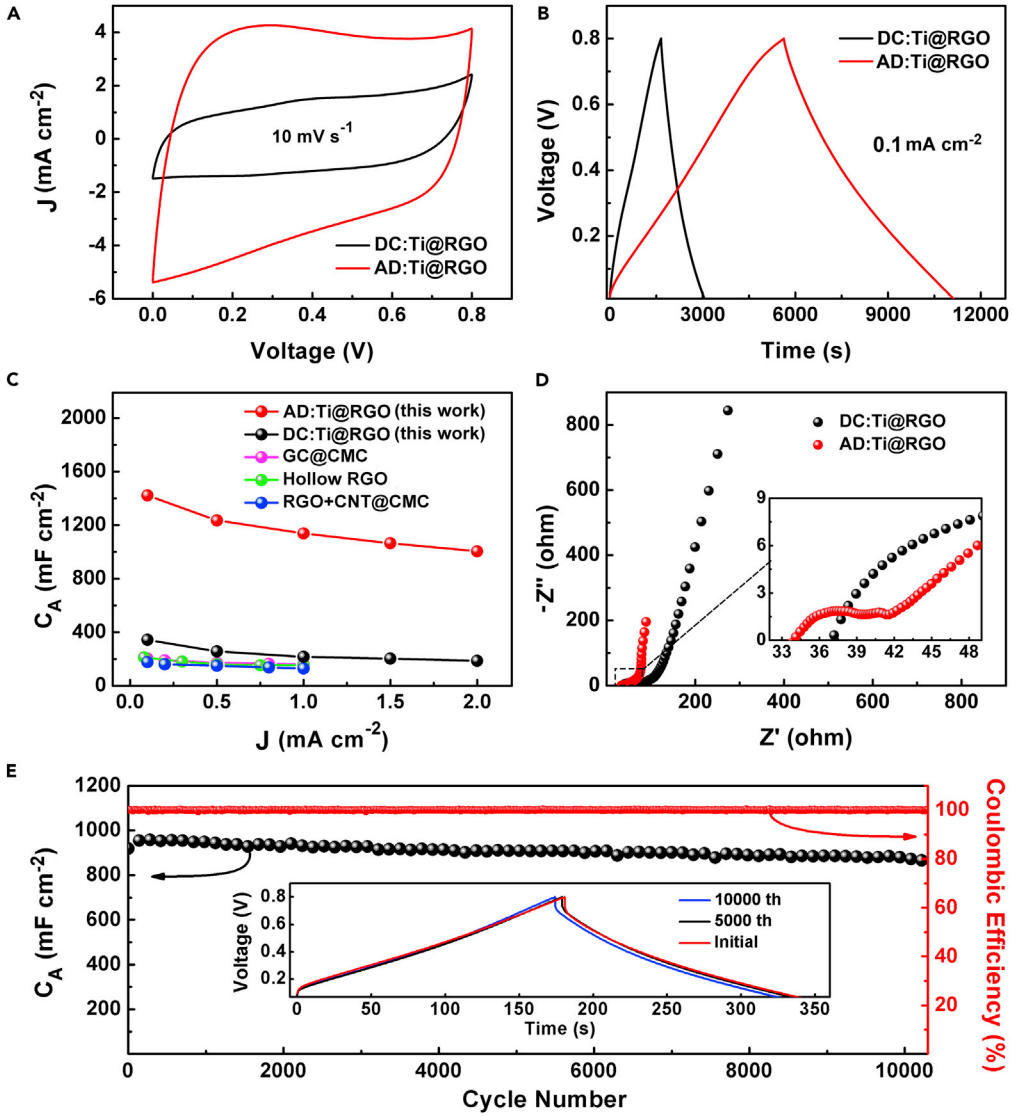

Figure 2. Electrochemical Performance of the AD:Ti@RGO- and the DC:Ti@RGO-Based FSCs

(A) CV curves of the AD:Ti@RGO- and the DC:Ti@RGO-based FSCs.

(B) GCD profiles of the AD:Ti@RGO- and the DC:Ti@RGO-based FSCs.

(C) C_A at increasing current densities of different FSCs. GC@CMC (Cai et al., 2017); hollow RGO (Qu et al., 2016); RGO + CNT@CMC (Kou et al., 2014).

(D) EIS with increasing frequencies from 100 kHz to 10 mHz.

(E) Long-term cycling stability of the AD:Ti@RGO at 2 mA cm^{-2} (inset: GCD profiles at the first, 5,000th, and 10,000th cycles).

explored as current collector (Purkait et al., 2018; Hu et al., 2016), they may not be the best core materials for FSCs as they could be readily oxidized during the supercapacitor operation (Figure S4). All-solid-state parallel FSCs (Figure S5) are assembled and tested by cyclic voltammetry (CV), galvanostatic charge-discharge (GCD), and electrochemical impedance spectroscopy (EIS).

Figure 2A presents the CV curves of the FSCs based on the AD:Ti@RGO and the DC:Ti@RGO, respectively, at a scanning rate of 10 mV s^{-1} with a potential range from 0 to 0.8 V. Both the AD:Ti@RGO-based and the DC:Ti@RGO-based FSCs display typical capacitive CV curves without apparent redox peaks, indicating a typical behavior of electrochemical double-layer capacitor (Ji et al., 2014). In the CV profiles, the AD:-Ti@RGO-based FSCs show a much larger integrable area than the DC:Ti@RGO-based FSCs,

demonstrating the much higher capacitance. GCD profiles taken at current density 0.1 mA cm^{-2} for both FSCs exhibit a typical triangular shape without any plateau (Figure 2B). This near-linear correlation between potential and time further verifies the double-layer-capacitor behavior of the FSCs. The symmetry between charge and discharge curves indicates a high Coulombic efficiency. At the same current densities of 0.1 mA cm^{-2}, the AD:Ti@RGO-based FSCs show a discharge time as long as 5,484.7 s, whereas the DC:Ti@RGO-based FSCs discharge for only 1,397.0 s. CV curves and GCD profiles taken at various scan rates and current densities are shown in Figure S6. Both FSCs retain quasi-rectangular CV curves even at a high scan rate of 100 mV s^{-1} and show no obvious voltage drops in GCD profiles until the current density rises to 1.0 mA cm^{-2}, indicating desirable rate performances. Figure 2C compares the capacitance of the AD:Ti@RGO FSCs at different current densities with those of previously reported advanced FSCs (Qu et al., 2016; Kou et al., 2014; Cai et al., 2017). As the surface area of human body for wearable electronics is limited, the areal specific capacitance and energy and power densities are particularly important for consideration (Beidaghi and Gogotsi, 2014).The DC:Ti@RGO has a specific areal capacitance (C_A) of 343.7 mF cm^{-2} at 0.1 mA cm^{-2}. The AD:Ti@RGO with diameter similar to that of DC:Ti@RGO possesses an ultra-high C_A of 1,442.2 mF cm^{-2}, which is ~3 times that of the high-cost UHMWPE/PDA/Ag/PEDOT composite fiber (563 mF cm^{-2}) (Du et al., 2018), 5 times that of the newly developed $Ti_3C_2T_x$ MXene-based fiber (328 mF cm^{-2}) (Hu et al., 2017), 28 times that of the typically pseudocapacitive CNT@Co_3O_4 fiber (52 mF cm^{-2}) (Su et al., 2015), and 1,000 times that of the similar neat graphene fiber (1.2–1.7 mF cm^{-2}) (Meng et al., 2013). A broader comparison of the C_A of AD:Ti@RGO with those of other neat graphene fibers can be seen in Figure S7. The corresponding length capacitance (C_L) and volume capacitance (C_V) of the AD:-Ti@RGO are 98.7 mF cm^{-1} and 257.4 mF cm^{-3}, respectively, which are also much higher than those of previously reported fibers (Figures S7 and S8A). Moreover, the AD:Ti@RGO-based FSCs can maintain a high C_A of more than 1,000 mF cm^{-2} even at current density as high as 2.0 mA cm^{-2}. Such satisfactory rate property may be ascribed to the conducting Ti wire current collector. The important role of the conducting Ti wire could be also seen in the EIS (Figure 2D). The equivalent series resistances of AD:Ti@RGO-based and DC:Ti@RGO-based FSCs (an analog to the internal resistance for a battery) are only 34.1 and 37.1 Ω, respectively. Supercapacitors exhibit a transition from resistance character into capacitance feature as frequencies shift from high to low (Taberna et al., 2003). Figure S9 presents the corresponding frequency dependence of the imaginary and real parts (C″ and C′) of the capacitance of the two FSCs. The C″ corresponds to energy dissipation by irreversible processes, whereas the C′ is an indicator of the capacitance of the supercapacitor devices (Taberna et al., 2003). It can be seen that AD:Ti@RGO-based FSCs show much higher C′ than DC:Ti@RGO-based FSCs at low frequency, in agreement with the result measured by constant-current discharge. The relaxation time constant (τ_0) is 46.4 s for AD:Ti@RGO-based FSCs and 21.5 s for DC:Ti@RGO-based FSCs, indicating longer discharge time required for the former due to its ultra-high capacitance. Moreover, AD:Ti@RGO-based FSCs also exhibit excellent cycling stability. As shown in Figure 2E, the C_A retention ratio of AD:Ti@RGO-based FSCs is 96% after 10,000 charge-discharge cycles at 2 mA cm^{-2}, accompanied by Coulombic efficiency of ≈100% for the whole course. The GCD profiles at initial, 5,000th, and 10,000th cycles are almost identical (Figure 2E inset), indicating the high electrochemical stability of AD:Ti@RGO.

Figure 3A shows the areal specific Ragone plots of different FSCs. Both the AD:Ti@RGO and DC:Ti@RGO fibers show relatively flat curves, indicating that their high energy density could be maintained during the increasing power output. The AD:Ti@RGO-based FSCs show a striking charge-storage capability with an ultra-high areal energy density (E_A) of 126.5 μW h cm^{-2} (based on one fiber electrode) or 31.6 μW h cm^{-2} (based on an entire FSC) at an areal power density (P_A) of 83.0 μW cm^{-2} or 20.8 μW cm^{-2}, correspondingly. As compared in Figure S7, the E_A of the AD:Ti@RGO is up to three orders of magnitude higher than those of previously reported neat graphene fibers. The corresponding volume specific Ragone plots are shown in Figure S8B. The volumetric energy density (E_V) of the AD:Ti@RGO is 22.9 mW h cm^{-3} at a volumetric power density (P_v) of 15.0 mW h cm^{-3}, which are about 2–12 times that of the most advanced composite fibers (2.16–12.7 mW h cm^{-3}) (Qu et al., 2016; Ma et al., 2015; Dong et al., 2014). Such high performances of the AD:Ti@RGO make it promising for practical applications. A cable-like FSC unit is made of two twisted AD:Ti@RGO at a length of about 3.5 cm (Figure 3A inset), by the fabrication processes shown in Figures 3B and S10. The CV curves and GCD profiles of the assembled FSC device made of one, two, or three FSC units connected in series are shown in Figure S11; both the CV curves and GCD profiles could well maintain their shape with potential window increasing, promising a capacity of practical application. Five FSC units connected in series as a supercapacitor bank can drive 27 LED lights (Figure 3C and Video S2). Five such supercapacitor banks connected in parallel can power a smart bracelet that used to be

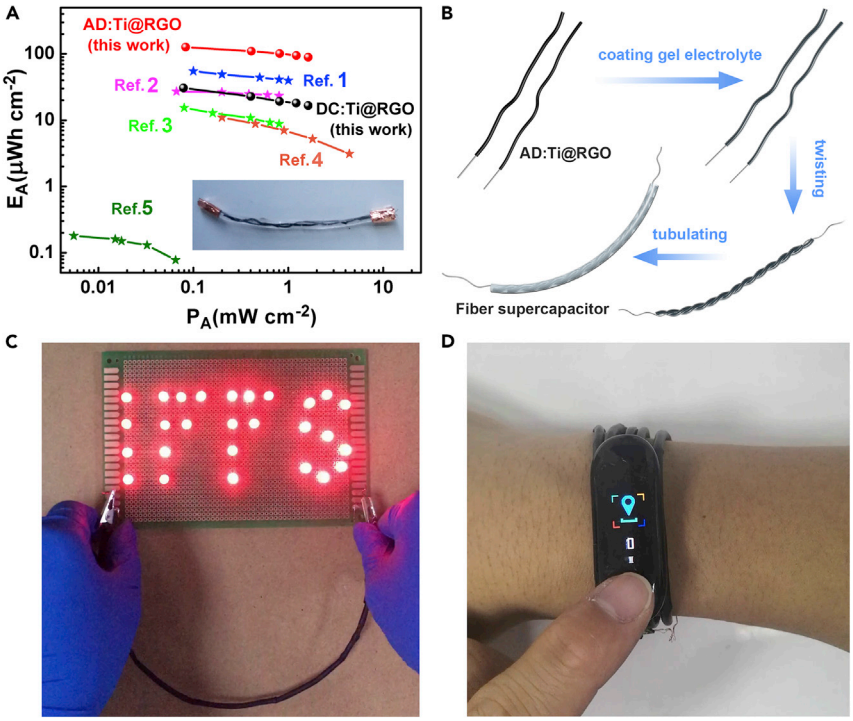

Figure 3. Performance in Practical Applications of the AD:Ti@RGO-Based Supercapacitor Devices

(A) Comparison of the areal specific Ragone plots of different FSCs. Ref. 1 (Cai et al., 2017); Ref. 2 (Qu et al., 2016); Ref. 3 (Kou et al., 2014); Ref. 4 (Le et al., 2013); Ref. 5 (Meng et al., 2013).

(B) Illustration of FSC fabrication.

(C) Photograph of a fiber-like flexible AD:Ti@RGO-based supercapacitor device to power 27 LEDs.

(D) Photograph of five fiber-like flexible AD:Ti@RGO-based supercapacitor devices as wearable band to power a smart bracelet.

powered by a high-energy-density lithium ion battery (Figures 3D and S12, and Video S3). These demonstrations directly evince in the candidacy of the AD:Ti@RGO-based FSCs for the wearable device applications.

Flexibility and Wear Resistance of the AD:Ti@RGO-Based FSCs

As the power source for wearable electronics, in addition to sufficiently high energy density and power density, the fibers must also possess excellent flexibility and wear resistance for extensive use. The flexibilities of the AD:Ti@RGO-based FSCs are systematically investigated by bending a flexible FSC into different angle. As shown in Figure 4A, the capacitances remained almost unchanged under bending with bending angles from 0° to 180° and then released to 0°. That the function of devices is not impacted by the bending of AD:Ti@RGO-based FSCs is demonstrated by an electronic wristband (Figure 4B) and a digital clock (Figure S13 and Video S4), evidencing the excellent flexibility. As tensile stress is also inevitable for wearable electronics, tensile resistance evaluations have been made. As shown in Figure S14, the CV curves of an AD:Ti@RGO-based FSC under a tensile stress and free state are almost overlapped. According the GCD profiles of the AD:Ti@RGO-based FSC before and after a tensile test (Figure S15), the capacitance loss is only about 2%, indicating the active material could bond well on the Ti fiber under a tensile stress. A long-term wear resistance test is further conducted by bending and straightening a flexible FSC for 500 cycles. The nearly unchanged CV curves of the FSC before and after bending 500 times indicate a considerable tolerance toward extensive wear and tear (Figure 4C). Figure 4D shows two AD:Ti@RGO-based FSCs being woven into textile fabric, demonstrating the good compatibility of AD:Ti@RGO-based FSCs and fabrics.

DISCUSSION

Graphene fibers suffer from the production limitation of special equipment, high manufacturing cost, unsatisfactory capacitance/energy density, etc., whereas the facilely prepared AD:Ti@RGO with high tensile

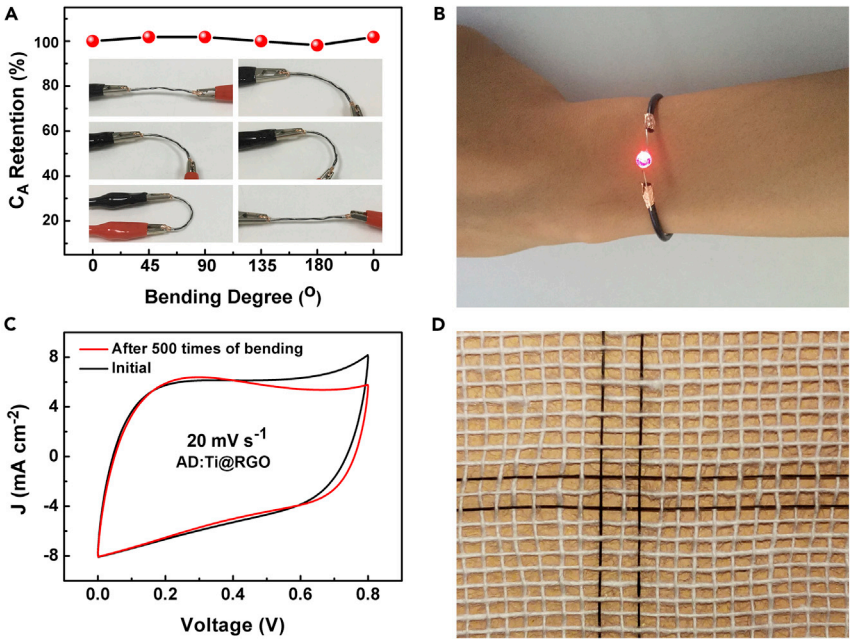

Figure 4. Wear Resistance and Flexibility of the AD:Ti@RGO-Based FSCs

(A) Capacitance retention of AD:Ti@RGO-based FSCs under different bending states.

(B) Photograph showing the wearability of a flexible AD:Ti@RGO-based FSC device.

(C) CV curves of a flexible AD:Ti@RGO-based FSC before and after bending for 500 times.

(D) Photograph of two AD:Ti@RGO-based FSCs being woven into textile fabric.

strength, great flexibility, excellent conductivity, and a striking enhancement by as high as three orders of magnitude in C_A and E_A versus that of conventional graphene fibers offer a promising power source candidate for future wearable devices.

The origin of the ultra-high capacitance of the AD:Ti@RGO is investigated. As the GO is prepared by Hummers' method with extensive use of potassium permanganate Hummers and Offeman, 1958, the possible contribution from manganese oxides is examined. The energy-dispersive X-ray spectroscopy element mapping (Figure S16) reveals a low Mn content in AD:Ti@RGO, implying that major capacitance is unlikely from the contribution of pseudo-capacitance from such small amount of manganese oxides. On the other hand, the excellent cycling stability of the AD:Ti@RGO-based FSCs also rules out the contribution from Mn species, because pseudo-capacitive materials, such as manganese oxides, usually show rapid capacity decay within several hundred cycles Chang et al., 2013. We believe the loosely stacked RGO sheets in AD:Ti@RGO may be responsible for the ultra-high capacitance as the book-pages-like yet interconnected structure may enable a significantly large effective surface area. As a supporting evidence, the C_A of the AD:Ti@RGO increases with increasing diameter (i.e., increasing mass loading of RGO by the repeating AD processes) of the AD:Ti@RGO (Figure S17). An ultra-high C_A up to 1,722.1 mF cm^{-2} at 0.1 mA cm^{-2} could be obtained by using thick AD:Ti@RGO. However, the mass-normalized specific capacitance (C_M) shows a volcano-like correlation to the diameter (i.e., loading) of the fiber, which is a result from the interplay between the increasing effective surface area and the increasing internal resistance (Figure S18). In contrast, the DC:Ti@RGO with densely stacked RGO sheets (Figures S19A and S19B), which lacks the space seen in AD:Ti@RGO (Figure S19C), may not allow the access of electrolyte and thus may not be available to provide additional capacitance (Figures S17 and S18). The effective surface areas of the two types of fibers are directly estimated by a CV method (Huang et al., 2017b). As shown in Figure S20, the specific surface areas of AD:Ti@RGO and DC:Ti@RGO are calculated to be 1.89 and 0.32 cm^2 g^{-1}, respectively, confirming that this AD method could bring large effective surface area.

Another major contribution to the ultra-high capacitance of the AD:Ti@RGO may be the abundant defects that are seen by Raman spectroscopy (Figure 1F). Previously reported RGO fibers are reduced by hydrothermal treatment, electrochemical reduction, AA, or hydroiodic acid, unlike the strongly alkaline

environment that is employed in preparation of AD:Ti@RGO. Zhang et al. have theoretically predicted that more defects may be generated on RGO in the presence of NaOH due to the diffusion of epoxies on the negatively charged graphene sheet (Chen et al., 2014b).The defects in RGO may induce pores, leading to increased charge-storage capability (Zhu et al., 2016). To verify the impact from strongly alkaline environment, AD:Ti@RGO fibers made in different coagulating and reducing solutions, including $CaCl_2$, NaOH, KOH, and ethanediamine, are compared (Figure S21). The AD:Ti@RGO made in neutral $CaCl_2$-based coagulating and reducing solution clearly underperforms compared with that made in various strongly alkaline solutions. On the other hand, the C_A of the AD:Ti@RGO made in $CaCl_2$ (692.4 mF cm^{-2} at 0.1 mA cm^{-2}) is still much higher than that of DC:Ti@RGO (343.7 mF cm^{-2} at 0.1 mA cm^{-2}), further confirming that the defects promoted by the alkaline processing environment is the secondary contribution to the ultra-high capacitance of AD:Ti@RGO, in addition to the proposed AD method itself.

Conclusion

In summary, we demonstrate a facile, scalable, and low-cost AD method to prepare RGO fibers that can be used to assemble FSCs for the next-generation power source of wearable devices. The as-prepared AD:Ti@RGO possesses high tensile strength, excellent conductivity, and great flexibility. Moreover, the AD:Ti@RGO-based FSCs show a record high capacitance of 1,722.1 mF cm^{-2}, which is up to three orders of magnitude higher than that of previously reported FSCs based on neat RGO fibers made by conventional methods. Ultra-high energy density of 126.5 μW h cm^{-2} (or 22.9 mW h cm^{-3}) could be achieved at power density of 83.0 μW cm^{-2} (or 15.0 mW h cm^{-3}). The high electrochemical performances could be well maintained after 10,000 cycles of operation and 500 times of bending, demonstrating the great stability and durability of AD:Ti@RGO-based FSCs. Practical applications are demonstrated by LED lights, digital display, and wearable smart bracelet. With their compatibility to fabrics, the AD:Ti@RGO-based FSCs offer a promising candidate for the power source of wearable devices, lighting the path to the next-generation technologies.

Limitations of the Study

The AD:Ti@RGO shows striking improvement in capacitance compared with previous neat RGO fibers. Although we have confirmed that the loose stack of RGO sheets and the defects resulted from alkaline treatment contribute to the high capacitance, the exact capacitance-increasing mechanism still needs to be further explored.

Resource Availability

Lead Contact

Further information and requests for resources and reagents should be directed to and will be fulfilled by the Lead Contact, Prof. Yijin Kang (kangyijin@uestc.edu.cn).

Materials Availability

This study did not generate new unique reagents.

Data and Code Availability

The materials that support the findings of this study are available from the corresponding authors upon reasonable request.

METHODS

All methods can be found in the accompanying Transparent Methods supplemental file.

SUPPLEMENTAL INFORMATION

Supplemental Information can be found online at https://doi.org/10.1016/j.isci.2020.101396.

ACKNOWLEDGMENTS

This work was financially supported by the National Natural Science Foundation of China (No. 21773023, 21972016, 51601030) and Sichuan Science and Technology Program (No. 2020YJ0243).

AUTHOR CONTRIBUTIONS

G.Q. and Y.K. conceived the idea. G.Q., Y.Z., J.Z., and L.X. carried out the materials synthesis and the electrochemical test. Y.K. supervised the project. G.Q. and Y.Z. contributed equally to this work. All authors discussed the results and wrote the manuscript.

DECLARATION OF INTERESTS

The authors declare no competing interests.

Received: February 10, 2020
Revised: June 12, 2020
Accepted: July 20, 2020
Published: August 21, 2020

REFERENCES

Bae, J., Park, Y.J., Lee, M., Cha, S.N., Choi, Y.J., Lee, C.S., Kim, J.M., and Wang, Z.L. (2011). Single-fiber-based hybridization of energy converters and storage units using graphene as electrodes. Adv. Mater. *23*, 3446–3449.

Beidaghi, M., and Gogotsi, Y. (2014). Capacitive energy storage in micro-scale devices: recent advances in design and fabrication of micro-supercapacitors. Energy Environ. Sci. *7*, 867–884.

Cai, S., Huang, T., Chen, H., Salman, M., Gopalsamy, K., and Gao, C. (2017). Wet-spinning of ternary synergistic coaxial fibers for high performance yarn supercapacitors. J. Mater. Chem. A *5*, 22489–22494.

Cao, Y., Zhu, M., Li, P., Zhang, R., Li, X., Gong, Q., Wang, K., Zhong, M., Wu, D., Lin, F., et al. (2013). Boosting supercapacitor performance of carbon fibres using electrochemically reduced graphene oxide additives. Phys. Chem. Chem. Phys. *15*, 19550–19556.

Cao, X., Yin, Z., and Zhang, H. (2014). Three-dimensional graphene materials: preparation, structures and application in supercapacitors. Energy Environ. Sci. *7*, 1850–1865.

Cao, X., Zheng, B., Shi, W., Yang, J., Fan, Z., Luo, Z., Rui, X., Chen, B., Yan, Q., and Zhang, H. (2015). Reduced graphene oxide-wrapped MoO_3 composites prepared by using metal–organic frameworks as precursor for all-solid-state flexible supercapacitors. Adv. Mater. *27*, 4695–4701.

Chang, J., Jin, M., Yao, F., Kim, T.H., Le, V.T., Yue, H., Gunes, F., Li, B., Ghosh, A., and Xie, S. (2013). Asymmetric supercapacitors based on graphene/MnO_2 nanospheres and graphene/MoO_3 nanosheets with high energy density. Adv. Funct. Mater. *23*, 5074–5083.

Chen, C., Kong, W., Duan, H.-M., and Zhang, J. (2014a). Theoretical simulation of reduction mechanism of graphene oxide in sodium hydroxide solution. Phys. Chem. Chem. Phys. *16*, 12858–12864.

Chen, C., Kong, W., Duan, H.M., and Zhang, J. (2014b). Theoretical simulation of reduction mechanism of graphene oxide in sodium hydroxide solution. Phys. Chem. Chem. Phys. *16*, 12858–12864.

Chen, D., Jiang, K., Huang, T., and Shen, G. (2019). Recent advances in fiber supercapacitors: materials, device configurations, and applications. Adv. Mater. *32*, 1901806.

Dong, Z., Jiang, C., Cheng, H., Zhao, Y., Shi, G., Jiang, L., and Qu, L. (2012). Facile fabrication of light, flexible and multifunctional graphene fibers. Adv. Mater. *24*, 1856–1861.

Dong, X., Guo, Z., Song, Y., Hou, M., Wang, J., Wang, Y., and Xia, Y. (2014). Flexible and wire-shaped micro-supercapacitor based on $Ni(OH)_2$-nanowire and ordered mesoporous carbon electrodes. Adv. Funct. Mater. *24*, 3405–3412.

Du, J., Wang, Z., Yu, J., Ullah, S., Yang, B., Li, C., Zhao, N., Fei, B., Zhu, C., and Xu, J. (2018). Ultrahigh-strength ultrahigh molecular weight polyethylene (uhmwpe)-based fiber electrode for high performance flexible supercapacitors. Adv. Funct. Mater. *28*, 1707351.

Gao, W., Emaminejad, S., Nyein, H.Y.Y., Challa, S., Chen, K., Peck, A., Fahad, H.M., Ota, H., Shiraki, H., and Kiriya, D. (2016). Fully integrated wearable sensor arrays for multiplexed in situ perspiration analysis. Nature *529*, 509.

Hu, M., Liu, Y., Zhang, M., Wei, H., and Gao, Y. (2016). Wire-type MnO2/Multilayer graphene/Ni electrode for high-performance supercapacitors. J. Power Sources *335*, 113–120.

Hu, M., Li, Z., Li, G., Hu, T., Zhang, C., and Wang, X. (2017). All-solid-state flexible fiber-based mxene supercapacitors. Adv. Mater. Technol. *2*, 1700143.

Huang, J., and Kaner, R.B. (2004). A general chemical route to polyaniline nanofibers. J. Am. Chem. Soc. *126*, 851–855.

Huang, T., Zheng, B., Kou, L., Gopalsamy, K., Xu, Z., Gao, C., Meng, Y., and Wei, Z. (2013). Flexible high performance wet-spun graphene fiber supercapacitors. RSC Adv. *3*, 23957–23962.

Huang, M., Wang, L., Chen, S., Kang, L., Lei, Z., Shi, F., Xu, H., and Liu, Z.-H. (2017a). Highly flexible all-solid-state cable-type supercapacitors based on Cu/reduced graphene oxide/manganese dioxide fibers. RSC Adv. *7*, 10092–10099.

Huang, D., Yang, Z., Li, X., Zhang, L., Hu, J., Su, Y., Hu, N., Yin, G., He, D., and Zhang, Y. (2017b). Three-dimensional conductive networks based on stacked SiO_2@graphene frameworks for enhanced gas sensing. Nanoscale *9*, 109–118.

Hummers, W.S., Jr., and Offeman, R.E. (1958). Preparation of graphitic oxide. J. Am. Chem. Soc. *80*, 1339.

Ji, Q., Zhao, X., Liu, H., Guo, L., and Qu, J. (2014). Facile synthesis of graphite-reduced graphite oxide core–sheath fiber via direct exfoliation of carbon fiber for supercapacitor application. ACS Appl. Mater. Interfaces *6*, 9496–9502.

Kim, J., Cote, L.J., Kim, F., Yuan, W., Shull, K.R., and Huang, J. (2010). Graphene oxide sheets at interfaces. J. Am. Chem. Soc. *132*, 8180–8186.

Kim, Y.S., Kang, J.H., Kim, T., Jung, Y., Lee, K., Oh, J.Y., Park, J., and Park, C.R. (2014). Easy preparation of readily self-assembled high-performance graphene oxide fibers. Chem. Mater. *26*, 5549–5555.

Kou, L., Huang, T., Zheng, B., Han, Y., Zhao, X., Gopalsamy, K., Sun, H., and Gao, C. (2014). Coaxial wet-spun yarn supercapacitors for high-energy density and safe wearable electronics. Nat. Commun. *5*, 3754.

Kudin, K.N., Ozbas, B., Schniepp, H.C., Prud'Homme, R.K., Aksay, I.A., and Car, R. (2008). Raman spectra of graphite oxide and functionalized graphene sheets. Nano Lett. *8*, 36–41.

Le, V.T., Kim, H., Ghosh, A., Kim, J., Chang, J., Vu, Q.A., Pham, D.T., Lee, J.-H., Kim, S.-W., and Lee, Y.H. (2013). Coaxial fiber supercapacitor using all-carbon material electrodes. ACS Nano *7*, 5940–5947.

Li, Y., Sheng, K., Yuan, W., and Shi, G. (2013). A high-performance flexible fibre-shaped electrochemical capacitor based on electrochemically reduced graphene oxide. Chem. Commun. *49*, 291–293.

Ma, Y., Li, P., Sedloff, J.W., Zhang, X., Zhang, H., and Liu, J. (2015). Conductive graphene fibers for wire-shaped supercapacitors strengthened by unfunctionalized few-walled carbon nanotubes. ACS Nano *9*, 1352–1359.

Meng, Y., Zhao, Y., Hu, C., Cheng, H., Hu, Y., Zhang, Z., Shi, G., and Qu, L. (2013). All-graphene core-sheath microfibers for all-solid-state, stretchable fibriform supercapacitors and

wearable electronic textiles. Adv. Mater. *25*, 2326–2331.

Purkait, T., Singh, G., Kumar, D., Singh, M., and Dey, R.S. (2018). High-performance flexible supercapacitors based on electrochemically tailored three-dimensional reduced graphene oxide networks. Sci. Rep. *8*, 640.

Qu, G., Cheng, J., Li, X., Yuan, D., Chen, P., Chen, X., Wang, B., and Peng, H. (2016). A fiber supercapacitor with high energy density based on hollow graphene/conducting polymer fiber electrode. Adv. Mater. *28*, 3646–3652.

Ren, J., Li, L., Chen, C., Chen, X., Cai, Z., Qiu, L., Wang, Y., Zhu, X., and Peng, H. (2013). Twisting carbon nanotube fibers for both wire-shaped micro-supercapacitor and micro-battery. Adv. Mater. *25*, 1155–1159.

Shao, Y., El-Kady, M.F., Wang, L.J., Zhang, Q., Li, Y., Wang, H., Mousavi, M.F., and Kaner, R.B. (2015). Graphene-based materials for flexible supercapacitors. Chem. Soc. Rev. *44*, 3639–3665.

Su, F., Lv, X., and Miao, M. (2015). High-performance two-ply yarn supercapacitors based on carbon nanotube yarns dotted with CoO and NiO nanoparticles. Small *11*, 854–861.

Sumboja, A., Foo, C.Y., Wang, X., and Lee, P.S. (2013). Large areal mass, flexible and free-standing reduced graphene oxide/manganese dioxide paper for asymmetric supercapacitor device. Adv. Mater. *25*, 2809–2815.

Taberna, P., Simon, P., and Fauvarque, J.-F. (2003). Electrochemical characteristics and impedance spectroscopy studies of carbon-carbon supercapacitors. J. Electrochem. Soc. *150*, A292–A300.

Xu, Z., and Gao, C. (2011). Graphene chiral liquid crystals and macroscopic assembled fibres. Nat. Commun. *2*, 571.

Xu, Z., and Gao, C. (2015). Graphene fiber: a new trend in carbon fibers. Mater. Today *18*, 480–492.

Xu, Y., Tao, Y., Zheng, X., Ma, H., Luo, J., Kang, F., and Yang, Q.H. (2015). A metal-free supercapacitor electrode material with a record high volumetric capacitance over 800 F cm^{-3}. Adv. Mater. *27*, 8082–8087.

Zhao, Y., Jiang, C., Hu, C., Dong, Z., Xue, J., Meng, Y., Zheng, N., Chen, P., and Qu, L. (2013). Large-scale spinning assembly of neat, morphology-defined, graphene-based hollow fibers. ACS Nano *7*, 2406–2412.

Zhao, F., Wang, Y., Xu, X., Liu, Y., Song, R., Lu, G., and Li, Y. (2014). Cobalt hexacyanoferrate nanoparticles as a high-rate and ultra-stable supercapacitor electrode material. ACS Appl. Mater. Inter. *6*, 11007–11012.

Zhu, J., Childress, A.S., Karakaya, M., Dandeliya, S., Srivastava, A., Lin, Y., Rao, A.M., and Podila, R. (2016). Defect-engineered graphene for high-energy- and high-power-density supercapacitor devices. Adv. Mater. *28*, 7185–7192.

iScience, Volume *23*

Supplemental Information

Alternately Dipping Method to Prepare Graphene Fiber Electrodes for Ultra-high-Capacitance Fiber Supercapacitors

Guoxing Qu, Yu Zhou, Jiahao Zhang, Lei Xiong, Qin Yue, and Yijin Kang

TRANSPARENT METHODS

Preparation of AD:Ti@RGO and DC:Ti@RGO. GO aqueous solution with a GO-content of 10 mg mL^{-1} used in this work was prepared by a Hummers' method and the details were described in a previous report (Marcano et al., 2010). 0.5 g of NaOH was dissolved in 10 mL of the mixture solution of deionized water and ethanol (1:4 in volume) to form coagulating solution. To make a reducing solution, 2 ml of the as-prepared coagulating solution was diluted by adding 10 mL of deionized water, followed by adding 0.05 g of ascorbic acid. Ti wire with a diameter of 100 μm was cut into desired length and then was cleaned by ultrasonication in ethanol and deionized water for 15 min in turn. To prepare AD:Ti@RGO, both the GO solution and coagulating solution was transferred into test tube-like containers and then the cleaned Ti wire is alternately dipped in the GO solution and the coagulating solution. As this alternately-dipping cycle repeats, GO precipitates are coated on the Ti wire layer by layer (see Supplementary Video 1). After drying, a chemical reduction is conducted in the reducing solution to reduce the coated GO to RGO at 85 ℃ for 4 h. The final AD:Ti@RGO was taken out after cooling down, washed with deionized water for more than 10 times before drying. To prepare DC:Ti@RGO, ascorbic acid was added to the GO solution with the weight ratios of 1:1, followed by an ultrasonic treatment to obtain a precursor solution. Then the as-prepared precursor solution was injected into glass pipes with a Ti wire in the center. Finally, the pipes were sealed and then placed in an oven at 85 ℃ for 4 h.

Fabrication of FSCs. To prepare a gel electrolyte, H_3PO_4 (~3 mL) and PVA powder (~3 g) were added into de-ionized water (~30 mL), followed by heating the mixture to

85-95 ℃ under vigorous stirring until it became clear. To obtain the electrochemical-performance parameters of AD:Ti@RGO and DC:Ti@RGO, parallel FSC was fabricated via fixing two same fibers on a substrate in parallel and then covering them with the H_3PO_4/PVA/H_2O gel electrolyte. To make wire-shape FSC, the electrode fibers was first coated with H_3PO_4/PVA/H_2O gel electrolyte. After drying, two AD:Ti@RGO electrodes with electrolyte coating are twisted together and then are coated with gel electrolyte again. Finally, the two twisted AD:Ti@RGO with electrolyte coating were put in a heat-shrink tube before shrinking the tube by heating.

Characterization. cyclic voltammetry (CV) and electrochemical impedance spectroscopy (EIS) measurements were performed on an electrochemistry workstation (CHI 760E, CH Instruments, US). Galvanostatic charge-discharge (GCD) profiles were tested using a CT-4008 battery program controlling test system (Neware, China). The scanning electron microscopy (SEM) images were taken by INSPECT-F50 (FEI, US). Raman spectrum was recorded on LabRAM HR Evolution (Horiba, France). The tensile stress-strain curves had been recorded from INSTRON8802 instrument (Instron, US).

Calculation of specific capacitance and energy density. The practical capacitance (C) of an entire FSC was calculated based on its GCD curves by the equation of $C = Q/U = I \times t/U$, where Q, U, I and t are the storage charge, voltage between two electrodes, discharge current and discharge time, respectively. For the convenience in comparison, specific capacitance (C_X) based on an individual fiber was used and calculated by $C_X = 2 \times C/X$ for a symmetric supercapacitor, where X could be surface area (A), effective

length (L), effective volume (V) or mass (M) for area-specific capacitance (C_A), length-specific capacitance (C_L), volume-specific capacitance (C_V) and mass-specific capacitance (C_M), respectively. The A and V are equal to the circumference and area of the cross-section of a fiber multiplied by the L (the length of overlapped portion of two electrodes), respectively. The practical energy (E) and power (P) of an entire supercapacitor could be obtained from $E = 0.5\times C\times U^2$ and $P = E/t$, respectively. In terms of specific energy (or energy density, E_X) and specific power (or power density, P_X), they could be obtained from $E_X = E/(2\times X)$ and $P_X = E_X/t$. Here "2" stands for the same two fiber electrodes in a symmetric supercapacitor. The areal energy density (E_A) may be calculated by $E_A = E/(2\times A) = 0.5\times C\times U^2/(2\times A) = 0.125\times(2\times C/A)\times U^2 = 0.125\times C_A\times U^2$. Some previous reports calculated energy density based on an individual fiber by using $E_A = 0.5\times C_A\times U^2$. For direct comparison with previous literature, both the specific capacitance and energy density was calculated on the basis of single fiber electrode if no particular statement is made in this work.

Evolution of the real and imaginary parts of electrochemical capacitance by EIS.

The frequency dependence of the real and imaginary parts (C' and C'')of electrochemical capacitance was obtained from EIS by using following equations:(Taberna et al.2003)

$$C'(\omega) = \frac{-Z''(\omega)}{\omega|Z(\omega)|^2}$$

$$C''(\omega) = \frac{Z'(\omega)}{\omega|Z(\omega)|^2}$$

where o is the angular frequency and Z' and Z'' are the real and imaginary parts of the impedance, defined as$Z'(\omega)^2 + Z''(\omega)^2 = Z(\omega)^2$

Estimation of effective surface area.

CV tests were carried out in the solution of 0.1 M KCl and 10 mM $K_3Fe(CN)_6$ to estimate the specific effective surface area of AD:Ti@RGO and DC:Ti@RGO, using a conventional three-electrode system. AD:Ti@RGO and DC:Ti@RGO served as the working electrode, a platinum gauze electrode a saturated calomel electrode (SCE) as the counter electrode and the reference electrode, respectively. The effective surface area can be calculated from the Randles−Sevcik equation.

$$I_p=(2.687\times10^5)n^{3/2}\nu^{1/2}D^{1/2}AC$$

Where I_p refers to the peak current, n is the number of electrons transferred in the redox process (n = 1, in 10 mM $K_3Fe(CN)_6$), ν is the scan rate, D is the diffusion coefficient (D= 5.7×10^{-6} cm^2 s^{-1}, in 0.1 M KCl), A is the surface area and C is the concentration of $K_3Fe(CN)_6$.

Video 1：the alternately dipping method. Related to Figure 1.

A fiber substrate was alternately dipped in GO solution and coagulation solution. As the cycle repeats, GO was coated on the fiber substrate gradually.

Video 2：powering 27 LED lights. Related to Figure 3.

A fiber-like supercapacitor device was made by serially connecting five AD:Ti@RGO-based FSCs with the length of about 3.5 cm each. The fiber-like supercapacitor device could drive 27 LED lights to emit bright light.

Video 3：powering a smart bracelet. Related to Figure 3.

A fiber-like supercapacitor device was made by serially connecting five AD:Ti@RGO-based

FSCs with the length of about 3.5 cm each. Five such fiber-like supercapacitor banks were connected in in parallel to power a smart bracelet.

Video 4：powering a digital clock. Related to Figure 4.

Three AD:Ti@RGO-based FSCs with the length of about 3.5 cm each were connected in parallel to form a unit. Then two such units were connected in series to form a FSC bank. A digital clock with large liquid crystal screen whose digits are as high as 1.5 cm was chosen as the appliance. The six FSCs were bended into 180 degree vertically to their axis. The bended FSC bank could power the electronic watch without any problem.

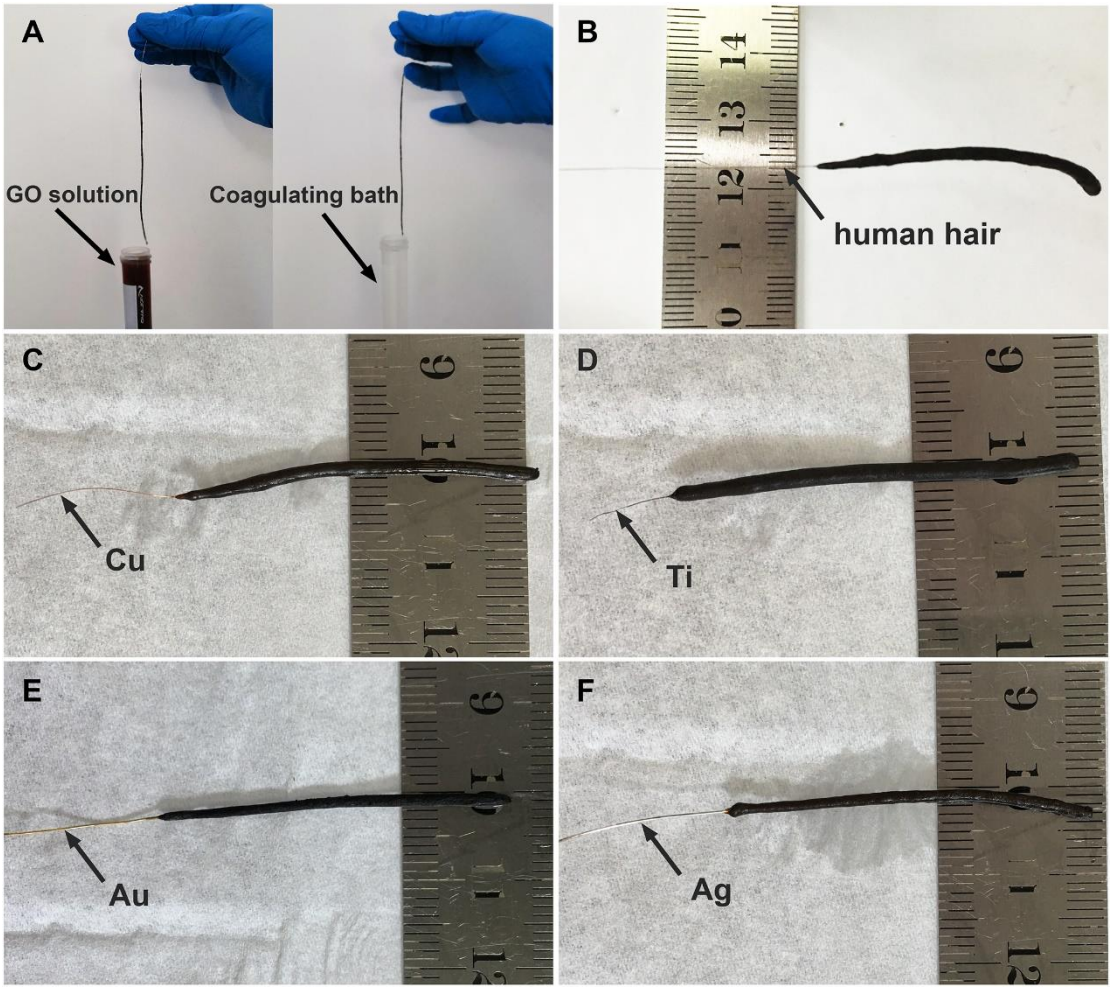

Figure S1. (A) Photograph of the alternately dipping method to coat GO on a fiber substrate. Photographs of coating GO on (B) human hair, (C) Cu wire, (D) Ti wire, (E) Au wire and (F) Ag wire substrate. Related to Figure 1.

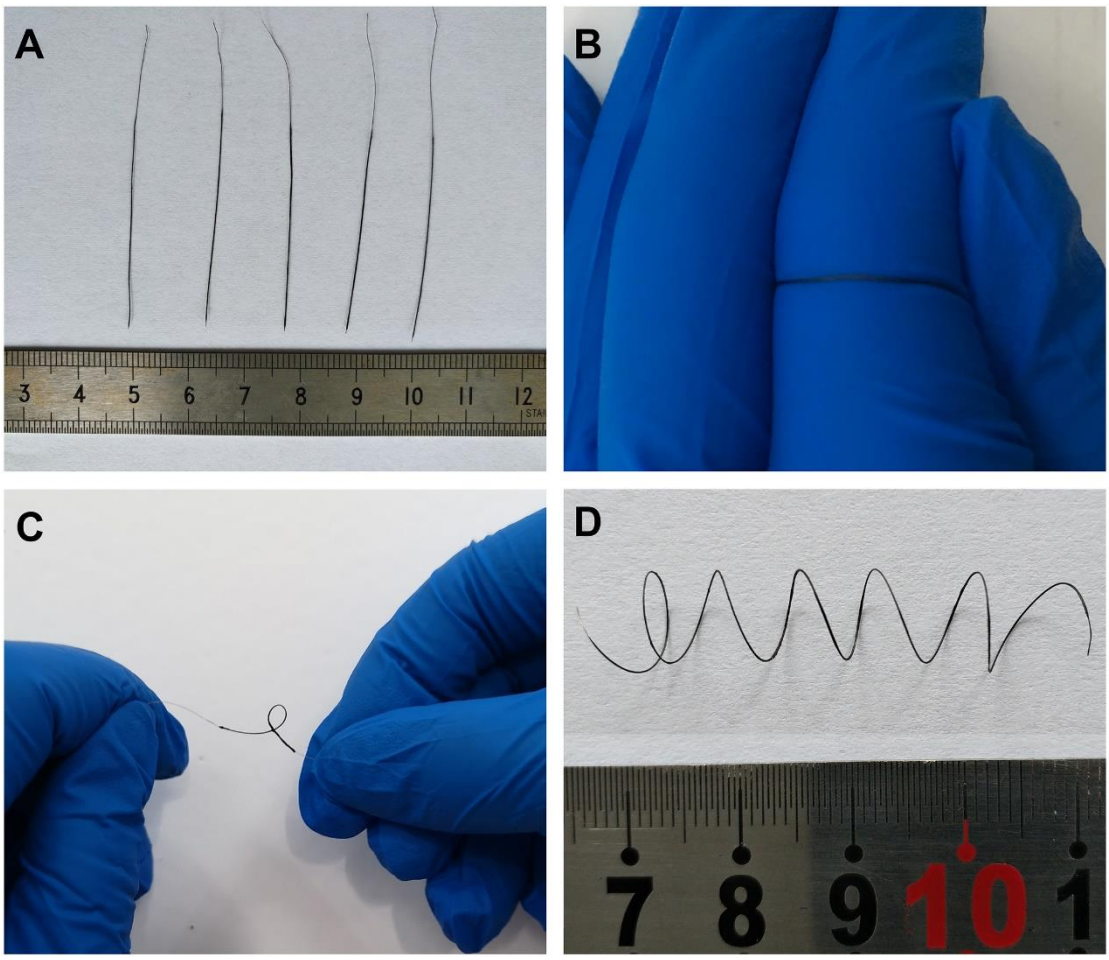

Figure S2. Photographs of (A) AD:Ti@RGO, (B) and (C) a bent AD:Ti@RGO to demonstrate its flexibility, (D) a long AD:Ti@RGO up to 15 cm, which was bent into a spring. Related to Figure 1.

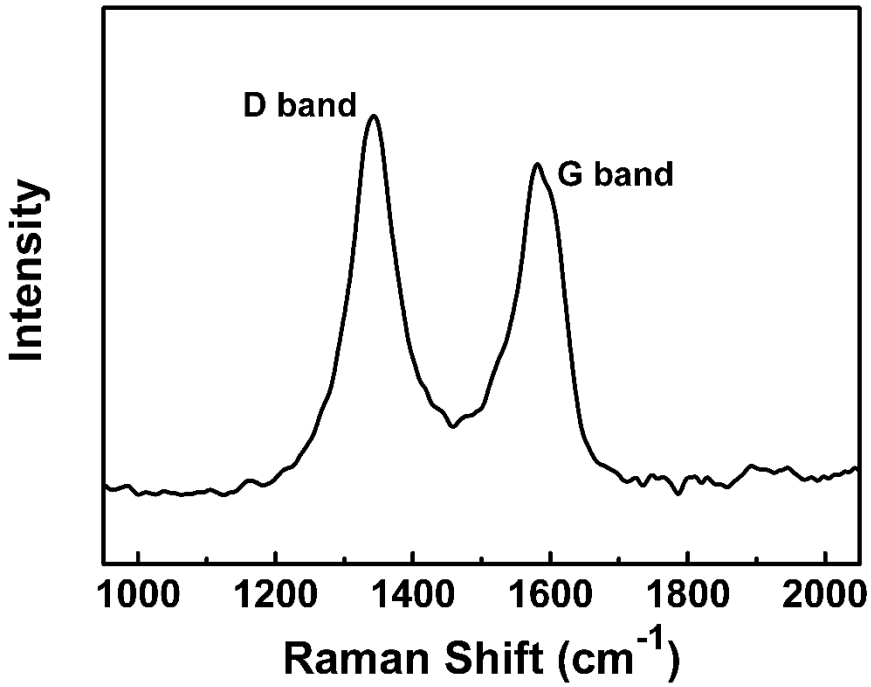

Figure S3. Raman spectrum of the DC:Ti@RGO. Related to Figure 1.

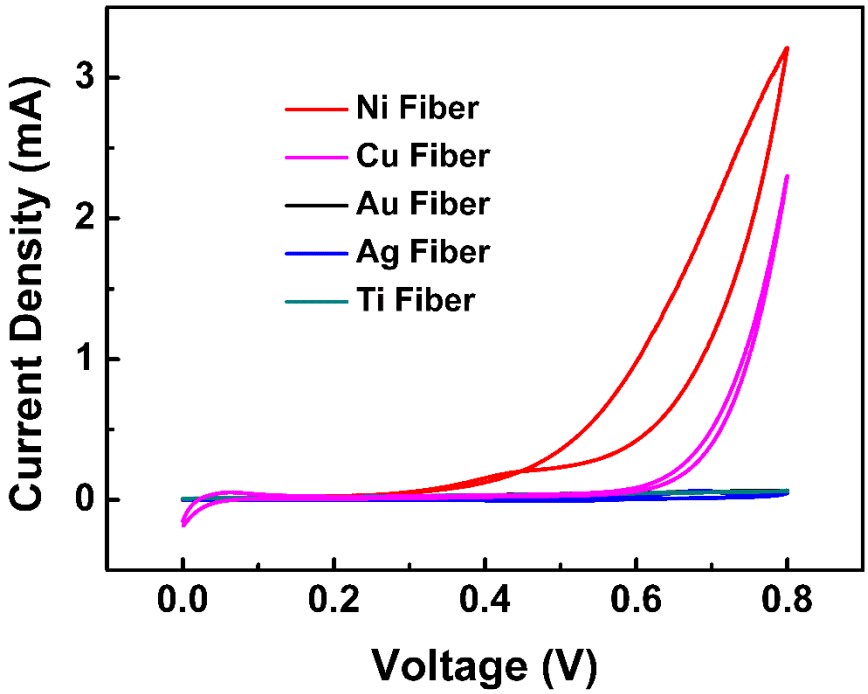

Figure S4. CV curves of different metal fiber substrate in H_3PO_4/PVA/H_2O gel electrolyte. Related to Figure 2.

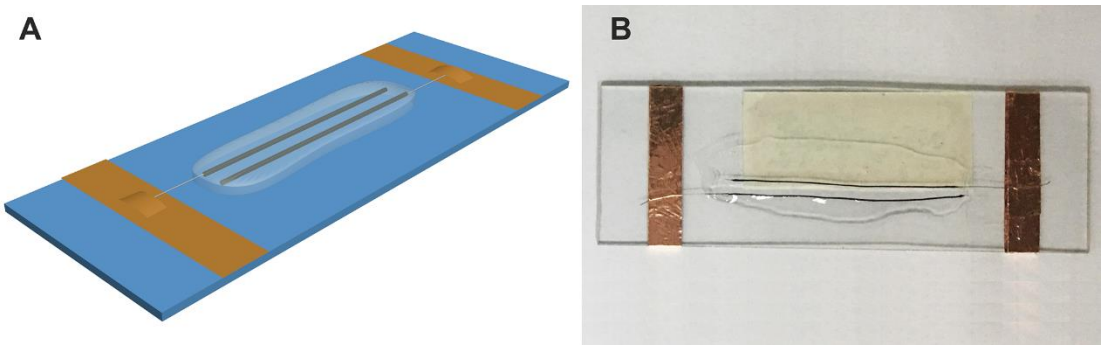

Figure S5. (A) The illustration of the all-solid-state parallel FSC. (B) Digital photograph of a parallel FSC. Related to Figure 2.

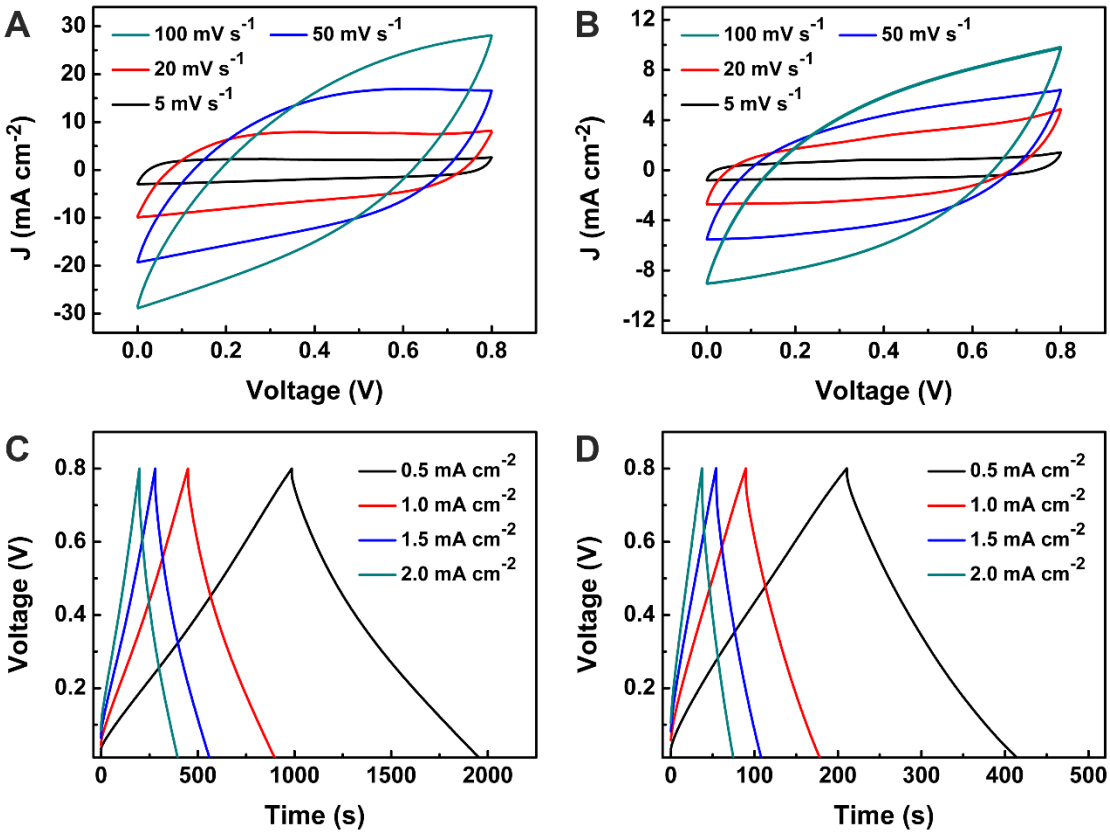

Figure S6. CV curves of (A) the AD:Ti@RGO-based FSCs and (B) the DC:Ti@RGO based FSCs at different scan rate. GCD profiles of (C) the AD:Ti@RGO-based FSCs and (D) the DC:Ti@RGO-based FSCs at different current density. Related to Figure 2.

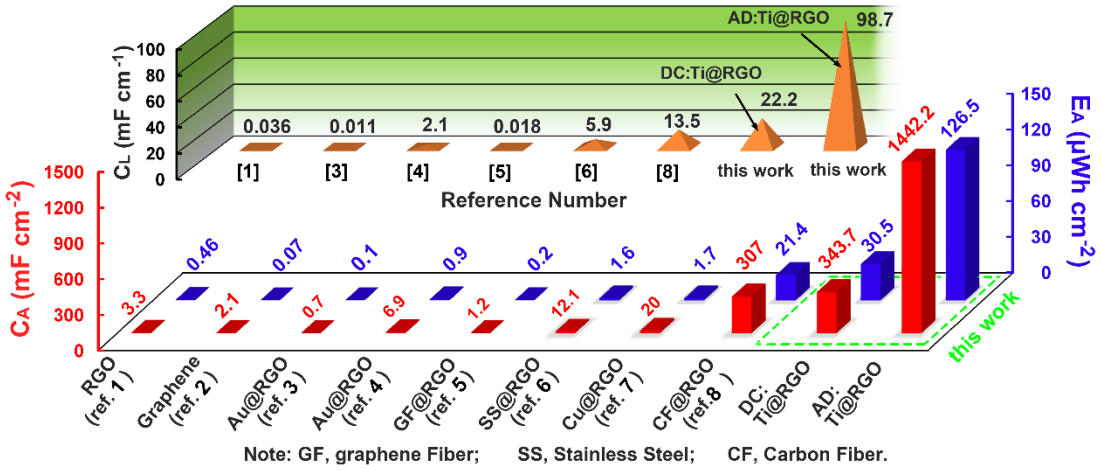

Figure S7. Comparison of the electrochemical performances of AD:Ti@RGO with the other neat graphene fiber in areal specific capacitance (C_A), length specific capacitance (C_L) and areal energy density (E_A). Ref. 1 (Huang et al., 2013); Ref. 2 (Li et al., 2013a); Ref. 3 (Li et al., 2013b); Ref. 4 (Chang et al., 2017); Ref. 5 (Meng et al., 2013); Ref. 6 (Veerasubramani et al., 2016); Ref. 7 (Huang et al., 2017); Ref. 8 (Cao et al., 2013). Related to Figure 2.

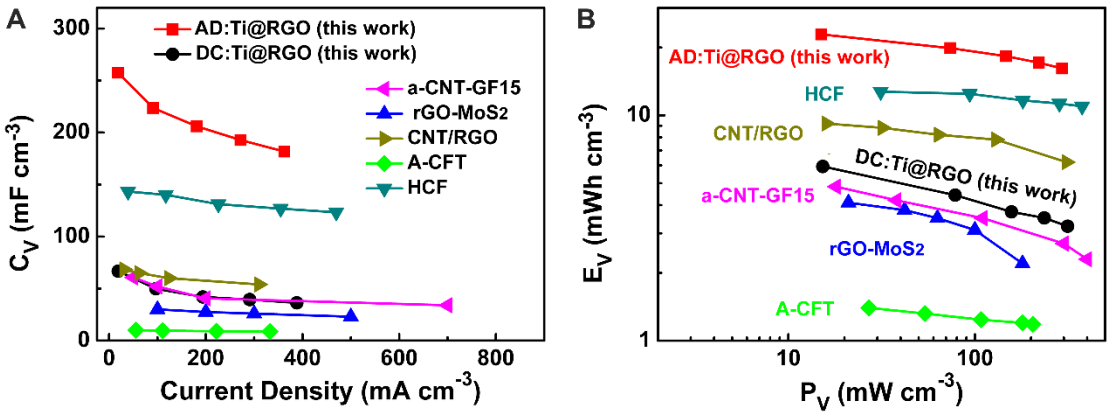

Figure S8. (A) Volume specific capacitances at increasing current densities of different FSCs. (B) Comparison of the volume specific Ragone plots of different FSC. a-CNT-GF15 (Park et al., 2019); rGO-MoS_2 (Sun et al., 2014); CNT/RGO (Wang et al., 2015); A-CFT (Yu et al., 2015); HCF (Qu et al., 2016). Related to Figures 2 and 3.

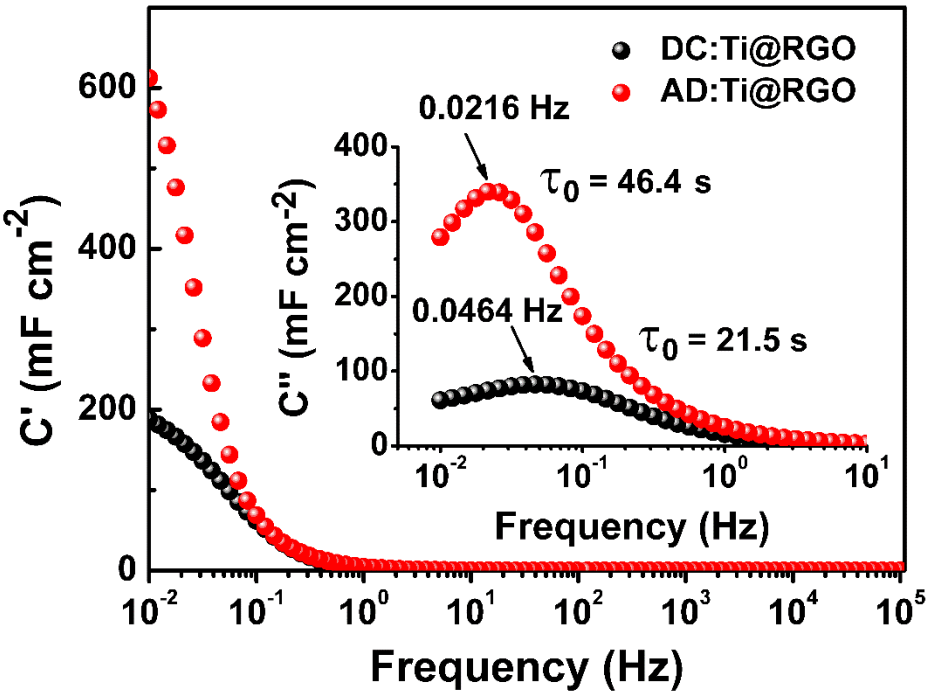

Figure S9. Frequency dependence of the real and imaginary parts (C' and C'') of the capacitance of the AD:Ti@RGO-based FSCs and the DC:Ti@RGO-based FSCs. Related to Figure 3.

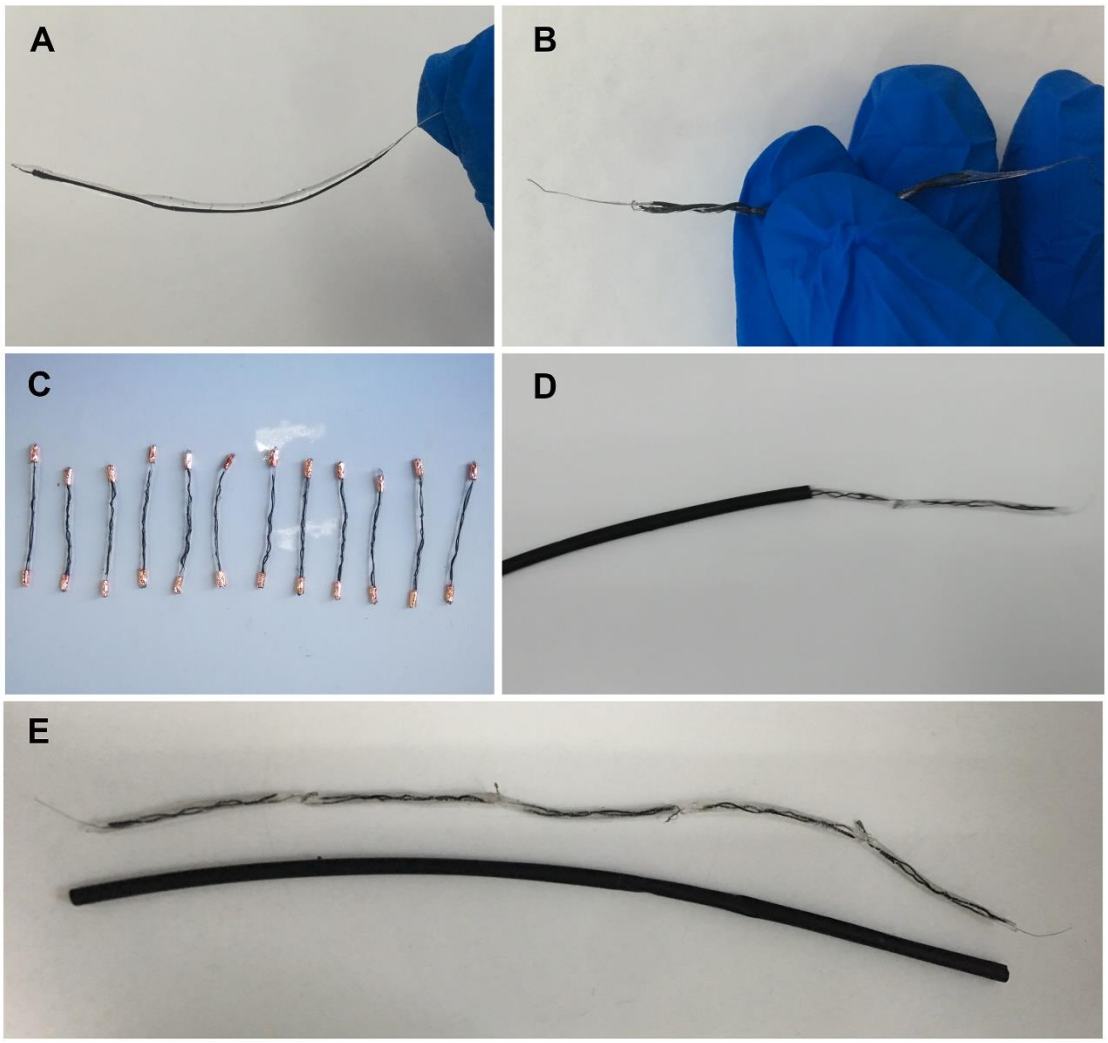

Figure S10. (A) Photograph of coating H_3PO_4/PVA/H_2O gel electrolyte on a fiber eletrode. (B) Photograph of two fiber electrodes coated with gel electrolyte being twisted together. (C) Photograph of as-assembled FSCs. (D) Photograph of inserting FSCs into a heat-shrink tube to make a fiber-like supercapacitor device. (E) Photograph of five FSC units connected in series and a heat-shrink tube with proper length. Related to Figure 3.

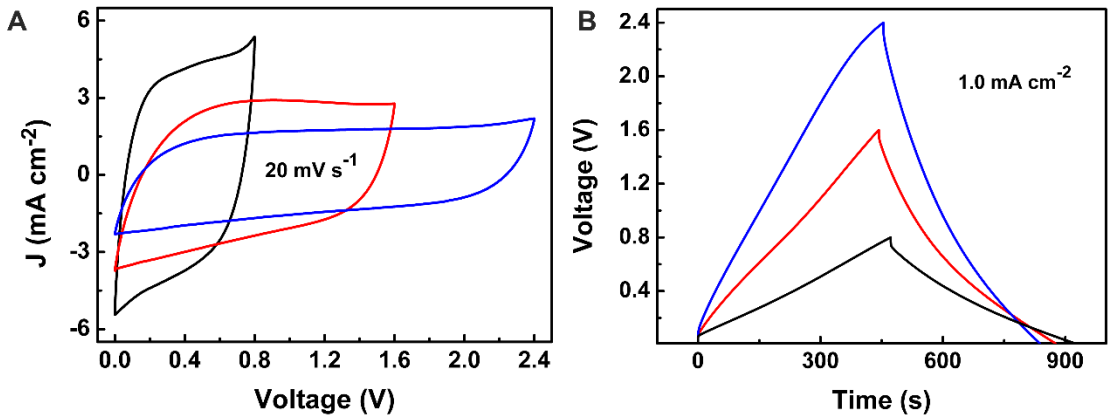

Figure S11. (A) CV curves and (B) GCD profiles of the assembled FSC device made of one, two or three AD:Ti@RGO-based FSC units connected in series. Related to Figure 3.

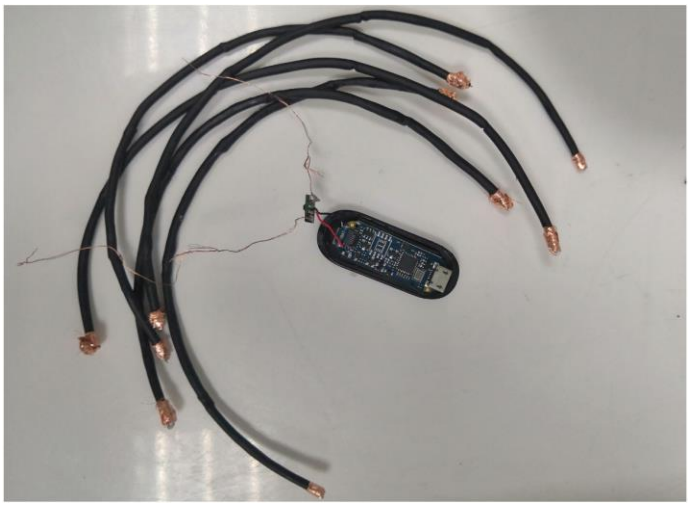

Figure S12. Photograph of the five fiber-like flexible AD:Ti@RGO-based supercapacitor banks and the reverse side of the smart bracelet. Related to Figure 3.

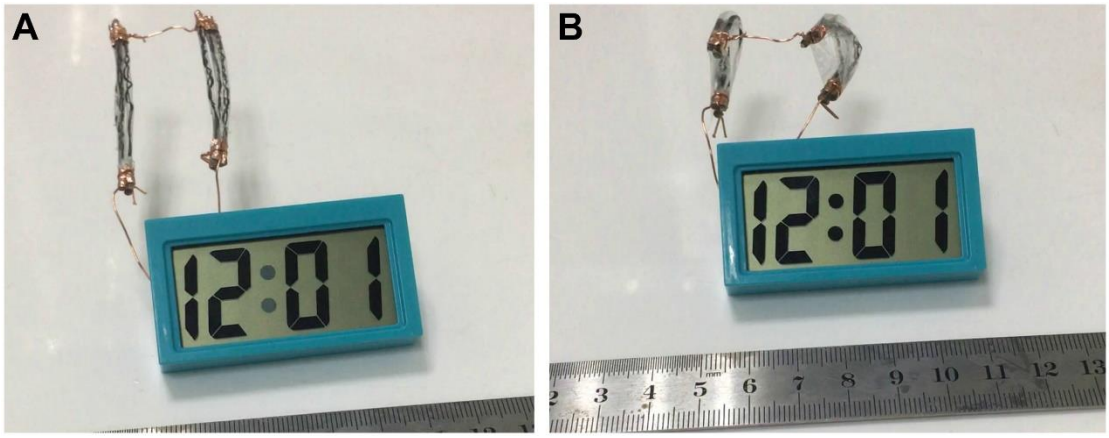

Figure S13. Photographs of six flexible AD:Ti@RGO-based FSCs (A) without bending and (B) under bending to power a digital clock. Related to Figure 4.

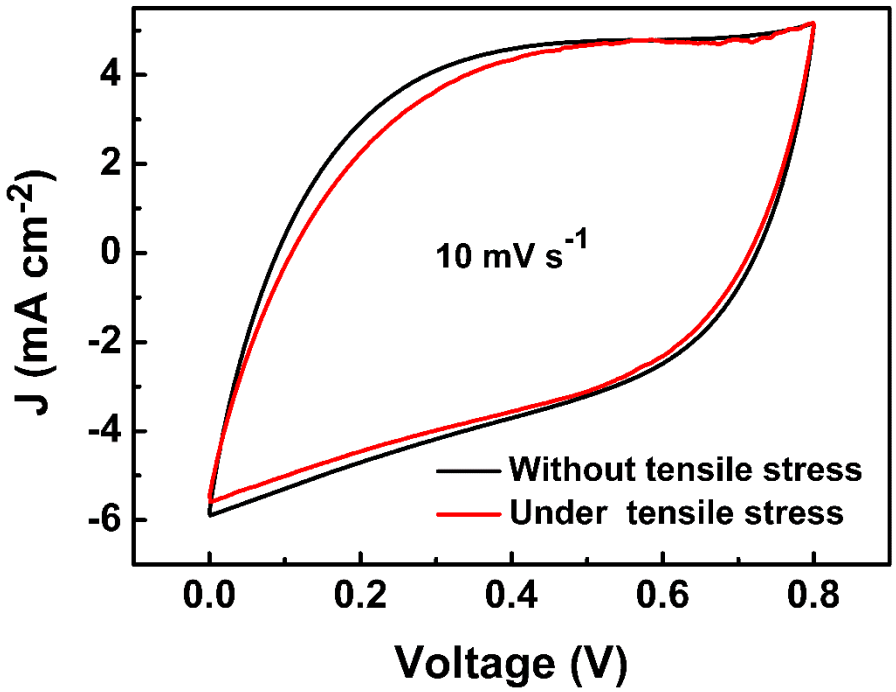

Figure S14. The CV curves of an AD:Ti@RGO-based FSC under a tensile stress and free state. Related to Figure 4.

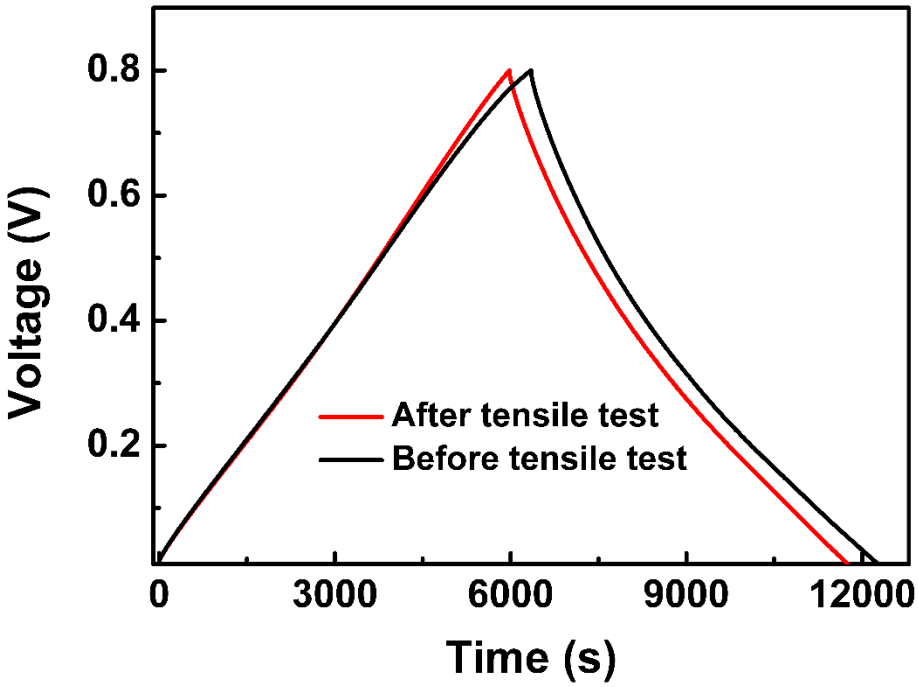

Figure S15. The GCD profiles of an AD:Ti@RGO-based FSC before and after a tensile test. Related to Figure 4.

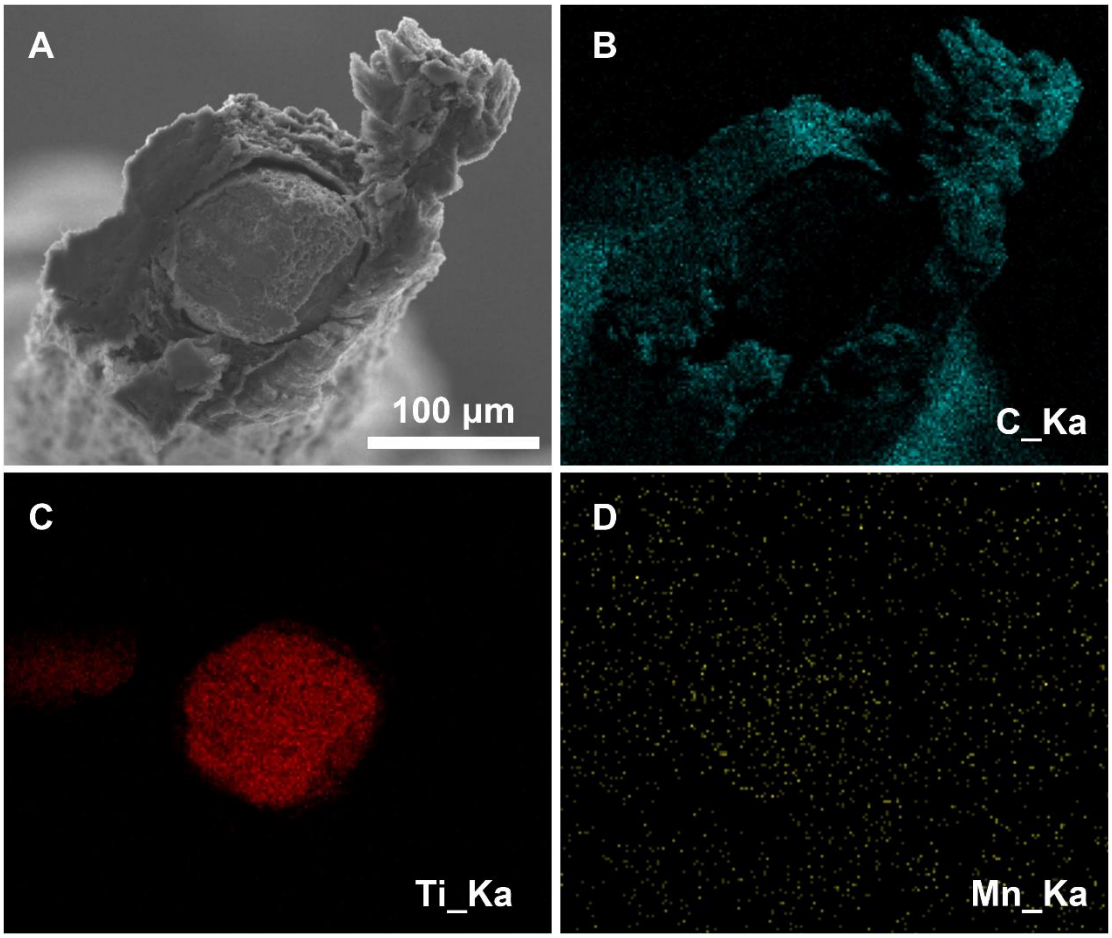

Figure S16. (A) Cross-sectional SEM images of the AD:Ti@RGO. Corresponding element distribution of (B) C element, (C) Ti element and (D) Mn element. Related to Figure 2.

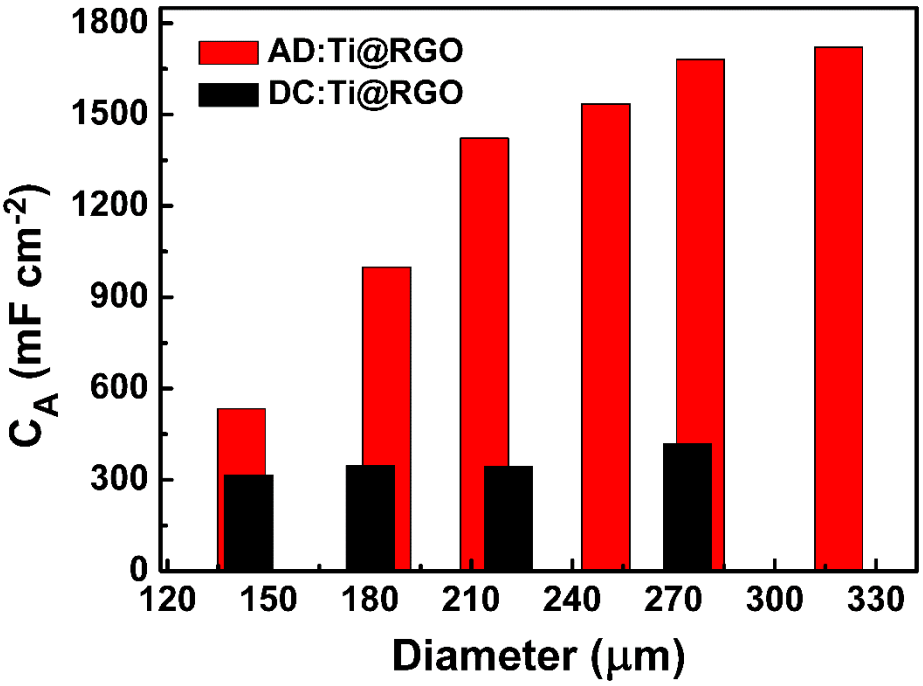

Figure S17. The correlation between areal specific capacitances at the current density of 0.1 mA cm^{-2} and the diameter of AD:Ti@RGO and DC:Ti@RGO. Related to Figure 2.

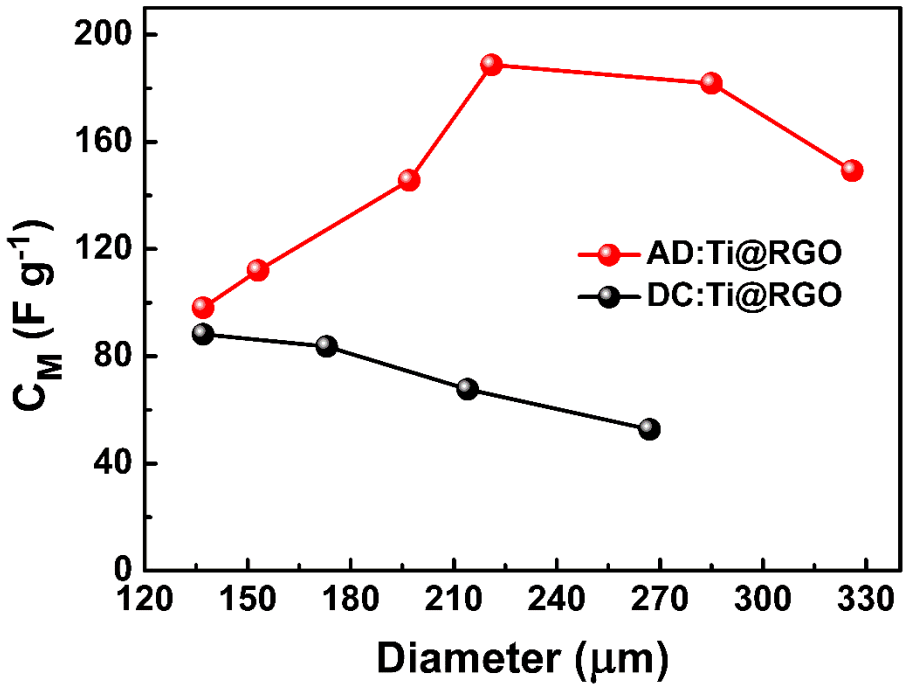

Figure S18. The correlation between mass specific capacitances at the current density of 0.1 mA cm^{-2} and the diameter of AD:Ti@RGO and DC:Ti@RGO. Related to Figure 2.

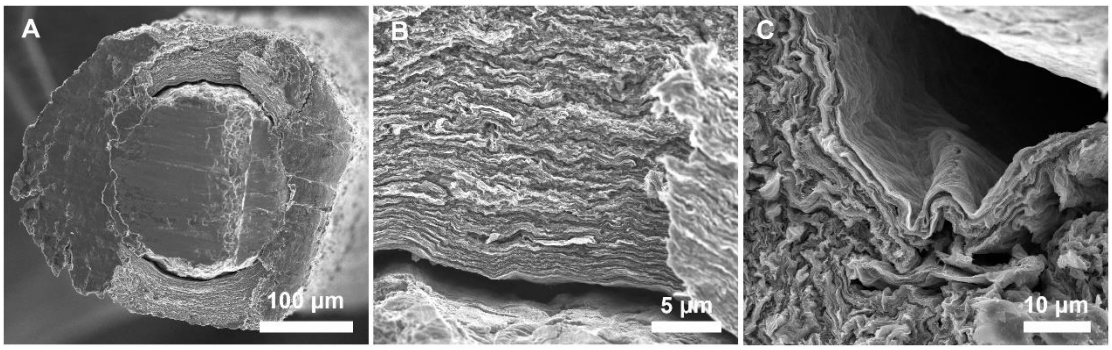

Figure S19. Cross-sectional SEM images of (A, B) the DC:Ti@RGO at different magnifications, and (C) the AD:Ti@RGO. Related to Figure 2.

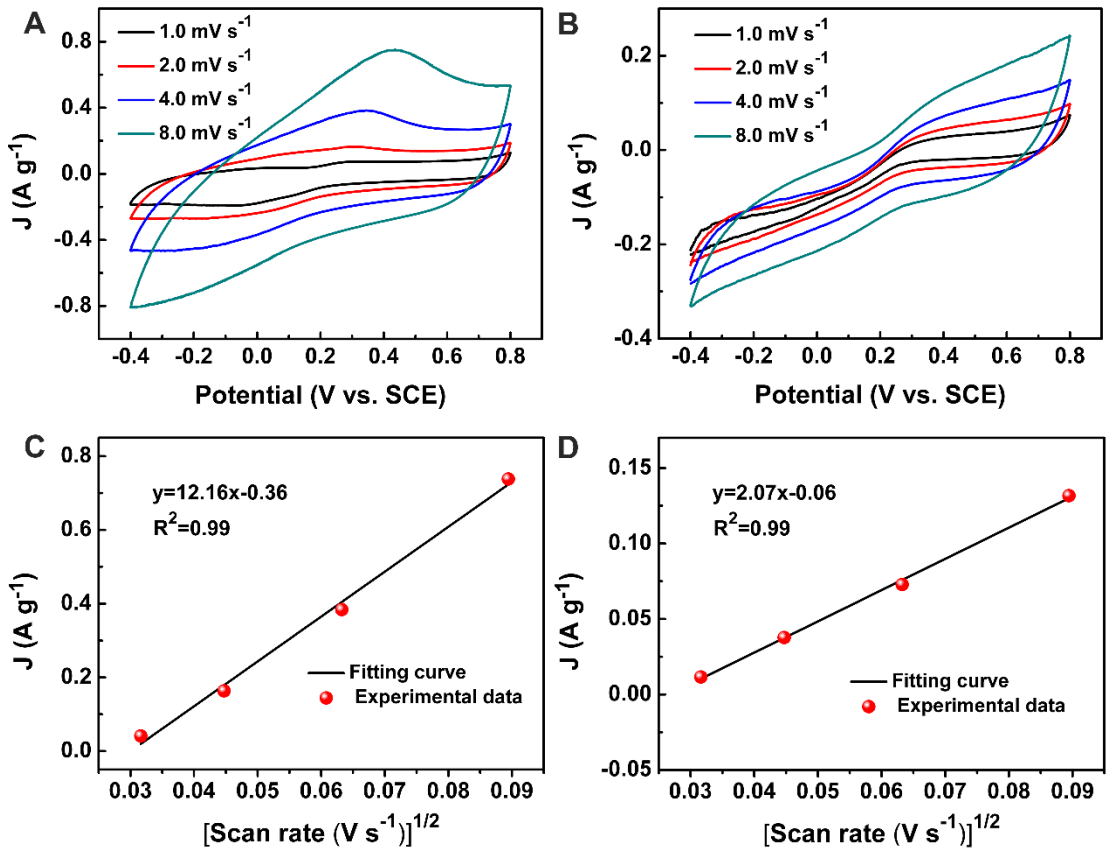

Figure S20. CV of (A) AD:Ti@RGO and (B) DC:Ti@RGO in a 10 mM $[Fe(CN)_6]^{3-/4-}$ and 0.1 M KCl solution at different scan rates. Peak currents as a function of scan rate for the determination of the effective surface area of (C) AD:Ti@RGO and (D) DC:Ti@RGO. Related to Figure 2.

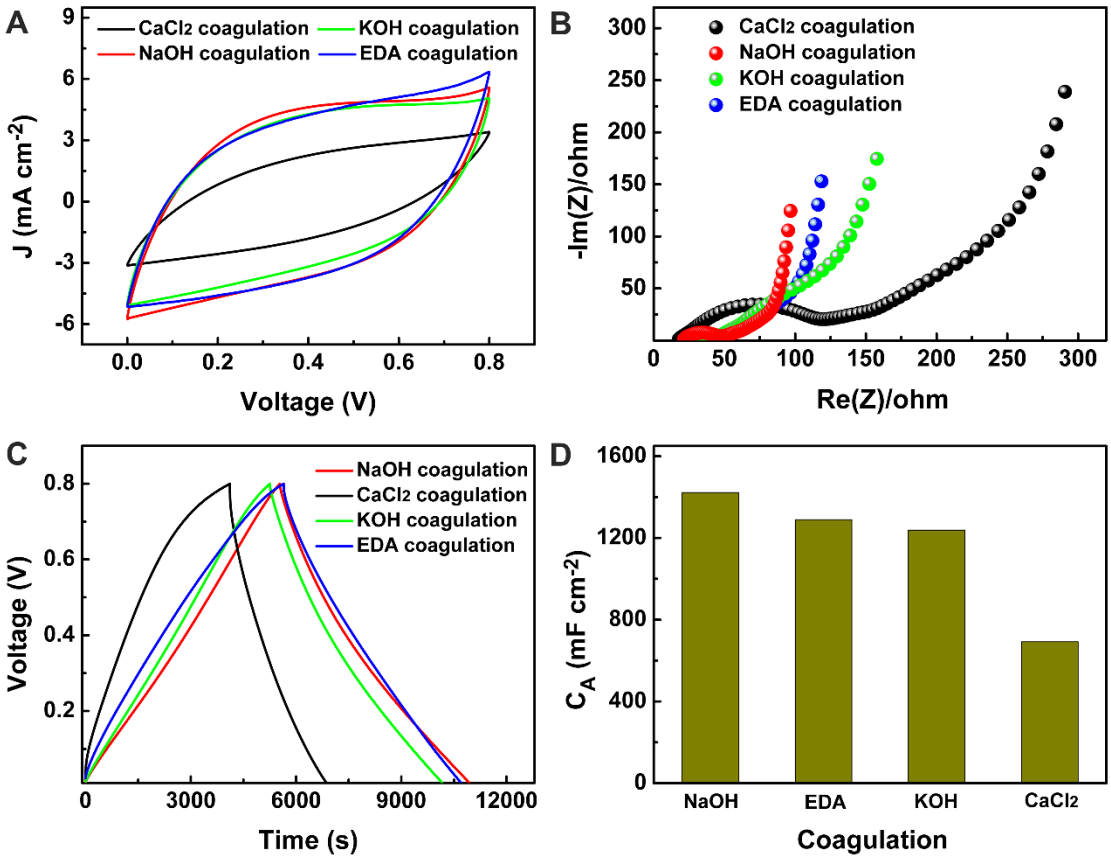

Figure S21. (A) CV curves at 20 mV s^{-1} of the FSCs based on AD:Ti@RGO made in different coagulation. (B) Corresponding electrochemical impedance spectra tested from 100 kHz to 10 mHz. (C) GCD profiles test at 0.1 mA cm^{-2} of the FSCs based on AD:Ti@RGO made in different coagulation. (D) Comparison of the areal specific capacitances of AD:Ti@RGO made in different coagulation. Related to Figure 2.

REFERENCES

Marcano, D.C., Kosynkin, D.V., Berlin, J.M., Sinitskii, A., Sun, Z., Slesarev, A., Alemany, L.B., Lu, W. and Tour, J.M. (2010). Improved synthesis of graphene oxide. ACS nano *4*, 4806-4814.

Taberna, P., Simon, P. and Fauvarque, J.-F. (2003). Electrochemical characteristics and impedance spectroscopy studies of carbon-carbon supercapacitors. J. Electrochem. Soc. *150*, A292-A300.

Huang, T., Zheng, B., Kou, L., Gopalsamy, K., Xu, Z., Gao, C., Meng, Y. and Wei, Z. (2013). Flexible high performance wet-spun graphene fiber supercapacitors. RSC Adv. *3*, 23957-23962.

Li, X., Zhao, T., Chen, Q., Li, P., Wang, K., Zhong, M., Wei, J., Wu, D., Wei, B. and Zhu, H. (2013a). Flexible all solid-state supercapacitors based on chemical vapor deposition derived graphene fibers. Phys. Chem. Chem. Phys. *15*, 17752-17757.

Li, Y., Sheng, K., Yuan, W. and Shi, G. (2013b). A high-performance flexible fibre-shaped electrochemical capacitor based on electrochemically reduced graphene oxide. Chem. Commun. *49*, 291-293.

Chang, Y.-z., Han, G.-y., Xiao, Y.-m., Zhou, H.-h., Li, M.-y., Fu, D.-y. and Zhou, W. (2017). High-performance flexible wire-shaped electrochemical capacitors based on gold wire@ reduced graphene oxide. New Carbon Materials *32*, 581-591.

Meng, Y., Zhao, Y., Hu, C., Cheng, H., Hu, Y., Zhang, Z., Shi, G. and Qu, L. (2013). All□Graphene Core□Sheath Microfibers for All□Solid□State, Stretchable Fibriform Supercapacitors and Wearable Electronic Textiles. Adv. Mater. *25*, 2326-2331.

Veerasubramani, G.K., Krishnamoorthy, K., Pazhamalai, P. and Kim, S.J. (2016). Enhanced electrochemical performances of graphene based solid-state flexible cable type supercapacitor using redox mediated polymer gel electrolyte. Carbon *105*, 638-648.

Huang, M., Wang, L., Chen, S., Kang, L., Lei, Z., Shi, F., Xu, H. and Liu, Z.-H. (2017). Highly flexible all-solid-state cable-type supercapacitors based on Cu/reduced graphene oxide/manganese dioxide fibers. RSC Adv. *7*, 10092-10099.

Cao, Y., Zhu, M., Li, P., Zhang, R., Li, X., Gong, Q., Wang, K., Zhong, M., Wu, D. and Lin, F. (2013). Boosting supercapacitor performance of carbon fibres using electrochemically reduced graphene oxide additives. Phys. Chem. Chem. Phys. *15*, 19550-19556.

Park, H., Ambade, R.B., Noh, S.H., Eom, W., Koh, K.H., Ambade, S.B., Lee, W.J., Kim, S.H. and Han, T.H. (2019). Porous graphene-carbon nanotube scaffolds for fiber supercapacitors. ACS Appl. Mater. Interfaces *11*, 9011-9022.

Sun, G., Liu, J., Zhang, X., Wang, X., Li, H., Yu, Y., Huang, W., Zhang, H. and Chen, P. (2014). Fabrication of Ultralong Hybrid Microfibers from Nanosheets of Reduced Graphene Oxide and Transition□Metal Dichalcogenides and their Application as

Supercapacitors. Angew. Chem. Int. Ed. *53*, 12576-12580.

Wang, B., Fang, X., Sun, H., He, S., Ren, J., Zhang, Y. and Peng, H. (2015). Fabricating continuous supercapacitor fibers with high performances by integrating all building materials and steps into one process. Adv. Mater. *27*, 7854-7860.

Yu, D., Zhai, S., Jiang, W., Goh, K., Wei, L., Chen, X., Jiang, R. and Chen, Y. (2015). Transforming pristine carbon fiber tows into high performance solid□state fiber supercapacitors. Adv. Mater. *27*, 4895-4901.

Qu, G., Cheng, J., Li, X., Yuan, D., Chen, P., Chen, X., Wang, B. and Peng, H. (2016). A Fiber Supercapacitor with High Energy Density Based on Hollow Graphene/Conducting Polymer Fiber Electrode. Adv. Mater. *28*, 3646-3652.